Chapter 3

Silicon Nanowires for Real-Time, Label-Free Biological Sensing

3.1 Introduction

Over the past few years a number of new biomolecular sensors have been reported.[1-5] The development of these devices is, in part, driven by the emerging needs of both systems biology[6, 7] and personalized and predictive medicine[8]–both of which are increasingly requiring quantitative, rapid, and multiparameter measurement capabilities on ever smaller amounts of tissues, cells, serum, etc. To meet these needs, many groups have focused their attention on developing real-time, highly sensitive and potentially scalable tools for detecting nucleic acids and proteins. One-dimensional nanostructures such as nanotubes,[9-12] semiconductor,[13-15] metal oxide nanowires (NWs),[16] and conducting polymer nanofilaments[17] have all been demonstrated as capable of the label-free detection of small molecules, nucleic acids, and proteins.

Silicon nanowire (SiNW) biosensors are promising label-free, electronic-based detectors of biomolecules.[2] However, significant scientific challenges remain before SiNW sensors can be viewed as a realistic technology. One challenge relates to the use of these devices in biologically relevant media, which is typically a 0.14M electrolyte. NW sensors detect the local change in charge density (and the accompanying change in

local chemical potential) that characterizes a target/capture agent binding event. That changing chemical potential is detected as a 'gating' voltage by the NW, and so, at a given voltage, affects the source (S) → drain (D) current value, or I_{SD}. However, that change is screened (via Debye screening) from the NW by the solution in which the sensing takes place.[18, 19] Debye screening is a function of electrolyte concentration, and in a 0.14M electrolyte (which represents physiological environments such as serum) the screening length is about 1 nm.[20] Because of this, all reports on SiNW sensors for proteins or DNA have been carried out in low ionic strength solutions.[14, 15, 21] In this chapter, we demonstrate that a single-stranded complementary oligonucleotide is able to significantly change the conductance of a group of 20 nm diameter SiNWs (p-doped at ~10^{19} cm^{-3}) in 0.165M solution by hybridizing to a primary DNA strand that has been electrostatically adsorbed onto an amine-terminated organic monolayer atop the NWs. This intimate contact of the primary strand with the amine groups of the NW surface brings the binding event close enough to the NW to be electronically detected. In addition, within a 0.165M ionic strength solution the DNA hybridization is more efficient.[10, 22] However, we further demonstrate that the sensing of proteins in physiological conditions is fundamentally limited by the size of the antibodies, which, at the moment, remain the most widely used high affinity probes for most proteins. This problem may be circumvented by utilizing alternative probes, such as aptamers.[12] Thus, if the antibodies are used as the probes for electrical label-free protein detection, the experiments are usually limited to low ionic strength solutions.

A second challenge involves demonstrating reproducible and high-throughput nanofabrication methods that can produce nearly identical NW sensors time and time again, and that allow for multiple measurements to be executed in parallel. Based on

electrostatic considerations, it is well known that nanowires are more sensitive to surface charges than planar ion-sensitive field-effect transistors (ISFET) or chemical field-effect transistor (CHEMFET). Such dimensional arguments[23] imply that nontraditional methods must be utilized to fabricate the NWs.[24, 25] While biological sensing with silicon produced by wet etch[26] or dry oxidation[27] was reported, to date, most reports of NW sensors have utilized semiconductor NWs grown as bulk materials[28] using the vapor-liquid-solid (VLS) technique.[29] This method produces high quality NWs, but they are characterized by a distribution of lengths and diameters, and they also must be assembled into the appropriate device structure (or the device structure must be constructed around the nanowire[30]). In this study we utilize the Superlattice Nanowire Pattern Transfer (SNAP) method[31] (chapter 2) to produce highly aligned array of 400 SiNWs, each 20 nm wide and ~2 millimeters long. Standard semiconductor processing techniques are utilized to control the NW doping level,[32] to section the NWs into several individual sensor arrays, to establish electrical contacts to the NW sensors, and to integrate each array into a microfluidic channel. Such integration is rather challenging in itself;[33] however, it is extremely important for obtaining low-noise, reproducible measurements. The resulting NWs exhibit excellent, controllable, and reproducible electrical characteristics from device to device and across fabrication runs. The sensor platforms may also be fabricated in reasonably high throughput. A key advantage which is provided by the top-down approach of SNAP versus the bottom-up VLS technique is the precise control of doping level of the nanowires. We utilize diffusion doping technique (chapter 2) to create nanowires with well characterized doping levels ranging from 10^{17} to 10^{20} cm^{-3}. We demonstrate that the doping level profoundly affects the limit

of detection of both DNA and protein; therefore, nanowires can be tuned to a specific dynamic range window with an appropriate concentration of impurities.

A third challenge involves the SiNW surface. The effectiveness of SiNWs for biomolecular sensing arises in part because of their high surface-to-volume ratio. The native (1-2 nm thick) surface oxide on a SiNW may limit sensor performance due to the presence of interfacial electronic states.[34, 35] In addition, the oxide surface of SiNWs acts as a dielectric which can screen the NW from the chemical event to be sensed. Covalent alkyl passivation of Si(111) surfaces can render those surfaces resistant to oxidation in air[36] and under oxidative potentials (chapter 4).[37, 38] Recently, methyl-passivated SiNWs were shown to exhibit improved field-effect transistor characteristics.[39] More complex molecules, such as amine terminated alkyl groups, can be covalently attached to H-terminated Si surfaces (including SiNWs) via UV-initiated radical chemistry.[40-43] Such chemistry has been used for a covalent attachment of DNA to VLS grown SiNWs.[44] DNA may also be immobilized on amine-terminated surfaces via electrostatic interactions. In this work, we explore how the characteristics of SiNW sensors vary as the nature of the inorganic/organic interface is varied. We find that SiNW sensors in which the native oxide provides the interface for organic functionalization are significantly inferior in terms of both sensitivity and dynamic range when compared with SiNW sensors that are directly passivated with an alkyl monolayer.

A final challenge is actually an opportunity that is provided by the intrinsic nature of a label-free, real-time sensor. The standard such sensing technique is surface plasmon resonance (SPR).[45] SPR is utilized to determine the κ_{on} and κ_{off} rates, and hence the equilibrium binding affinities, of complementary DNA strands or antibody-protein pairs.

The capture agent (single-stranded DNA or an antibody) is typically surface bound, and so the key experimental variables are the analyte (complementary DNA strand or a protein) concentration and time. If κ_{on} and κ_{off} are both known, then SPR can be utilized to quantitate the analyte concentration. Very few biomolecular sensing techniques are quantitative. In this work, dope the NW sensors so that their sensing dynamic range is optimized to match that of SPR for the detection of DNA hybridization or protein binding to an antibody. We demonstrate the equivalence of these two methods, and thus demonstrate the potential use of SiNW sensors for quantitating analyte concentrations. SiNW sensors can be optimized for significantly higher sensitivity than SPR by an appropriate surface modification and doping, and thus can potentially be utilized to quantitate the concentrations of specific biomolecules at very low concentrations. That would constitute a unique application of these devices.

3.2 Experimental Methods

3.2.1 Nanowire Sensor Fabrication

The SiNW arrays were fabricated as previously described,[46] and all fabrication was done within a class 1000 or class 100 clean room environment. A typical NW sensor device employed in this work for DNA sensing is shown in Figure 3.1. The starting material for the SNAP process was an intrinsic, 320 Å thick silicon-on-insulator (SOI) substrate with (100) orientation (Ibis Technology, Danvers, MA) and with a 1500 Å buried oxide. Cleaned substrates were coated with either p-type (Boron A, Filmtronics, Bulter, PA) or n-type (Phosphorosilica, Emulsitone, Whippany, NJ) spin-on-dopants (SODs). SODs were thermally diffused into the SOI film (chapter 2). We reproducibly controlled the resulting substrate doping concentration, as quantified by 4-point

resistivity measurements on the SOI film, by varying the diffusion temperature. The exact doping conditions, including the temperatures corresponding to particular doping levels, are described in details in chapter 2. The p-type substrates were thermally

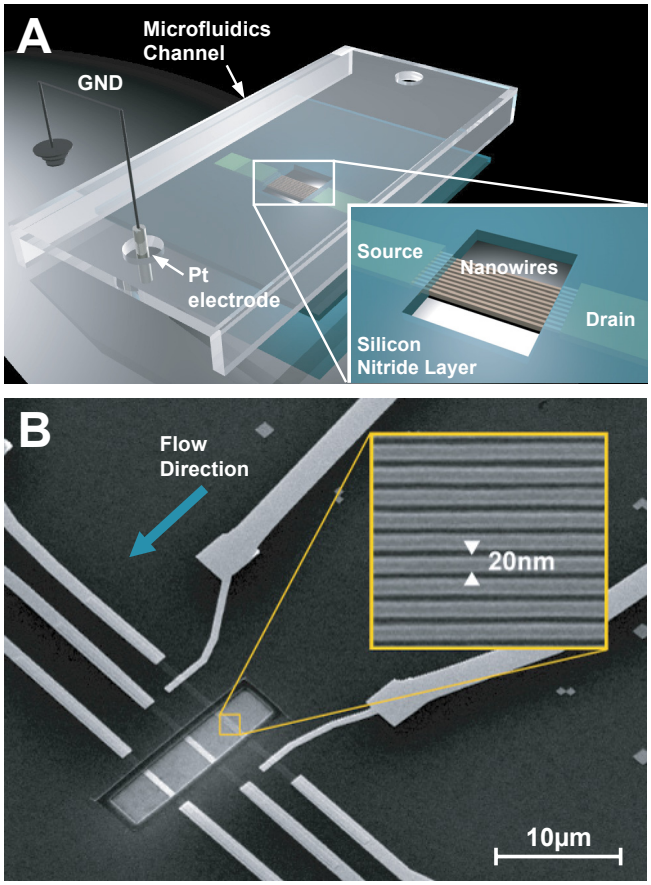

Figure 3.1: A diagram (A) and an SEM image (B) of a single device section containing three groups of ~10 SiNWs in a microfluidics channel. The wafer is covered with Si_3N_4 except for an exposed active region with SiNWs (A, inset; B). B, inset: High resolution SEM image of 20 nm SiNWs.

oxidized in O_2 for 1 minute at 850 ^oC, which was necessary to remove the organic SOD residue. The SOD films were removed by brief immersion in piranha (70% H_2SO_4, 30% H_2O_2), followed by a water rinse, and immersion in buffered oxide etchant (BOE; General Chemical, Parcippany, NJ).

The SNAP method for NW array fabrication translates the atomic control achievable over the individual layer thicknesses within an MBE-grown $GaAs/Al_xGa_{(1-x)}As$ superlattice into an identical level of control over NW width, length and spacing. This method has been described in some detail elsewhere,[31, 46] and will not be described here (refer to chapter 2 for details). We utilized the SNAP process to produce a 2 mm long array of 400 SiNWs, each of 20 nm width and patterned at 35 nm pitch (Figure 3.1B, inset).

The SiNWs were sectioned into ~30 μm long segments using e-beam lithography (EBL) and SF_6 RIE etching, producing groups of ~10 SiNWs with a diameter of 20 nm. Six identical sections from a single imprint, each containing 3 NW segments, were produced. One such section is shown in Figure 3.1. When fully integrated with the microfluidics channels, this allowed for six separate measurements, with three independent NW segments per measurement. Source (S) and drain (D) electrical contacts, ~500 nm wide and separated by 10-15 μm, were patterned using electron beam lithography (EBL) on each section of SiNWs. Prior to metallization, the native oxide of the SiNWs over the contacts was removed with BOE to promote the formation of ohmic contacts. Finally, 400 Å Ti and 500 Å Pt were evaporated to form S/D contacts. Immediately after the liftoff, the devices were annealed in 95% N_2, 5% H_2 at 475^{o}C for 5 minutes. This step greatly improves the characteristics of SNAP SiNW FETs. To provide room for a 1 cm by 1.5 cm PDMS chip with microchannels for analyte delivery to each section of the SiNWs (Figures 3.1A and 3.2), the electrical contacts were extended to the edges of the substrate using standard photolithography techniques followed by evaporation of 200 Å Ti and 1500 Å Au. To eliminate parasitic current between metal contacts in solution, approximately 70 nm of Si_3N_4 was deposited using

plasma-enhanced chemical vapor deposition (PECVD) everywhere on the chip except in 5 μm by 20 μm regions over the NWs and the outer tips of the Au contacts. Briefly, 100 nm of chromium was deposited over an active region of the NWs. PECVD was used to deposit Si_3N_4 film at 300°C (900mT, 20W, 13.5MHz) from N_2 (1960 sccm), NH_3 (55 sccm) and SiH_4 (40 sccm) gases. The nitride film was selectively etched with CHF_3/O_2 plasma over the protected NW region using PMMA as a mask, followed by the removal of chromium with CR-7C (Cyantek Corp., Fremont, CA).

Microfluidics fabrication. The soft lithography microfluidics chips were fabricated as described by others.[47] We observed that manual introduction/changing of solutions caused serious noise, capacitive currents and baseline shifts in real-time recordings. Thus, for low noise, stable real-time electronic measurements, we found it necessary to automate fluid injection and solution switching by using PDMS multilayer, integrated elastomeric microfluidics chips of the type developed by the Quake and Scherer groups.[48] The size of the wafer containing SiNWs did not permit the inclusion of all necessary flow and control lines necessary for the fluidic handling chip, and so that was fabricated as a separate chip. Such PDMS chip was fabricated using a standard photolithography: mixed PDMS (Dow Corning, Midland, MI) was applied over a premade photoresist (Shipley SPR 220-7) molding on silicon wafer and incompletely cured at 80 °C for 30 minutes. The chip containing microchannels was cut out of the PDMS layer and 0.5 mm diameter holes were punctured to serve as microchannel inlets and outlets. The fluidic chip and the device containing SiNWs were then brought into contact, with the 100μm wide microchannels aligned over the individual nanowire sections. The assembled device was cured to completion overnight at 80 °C.

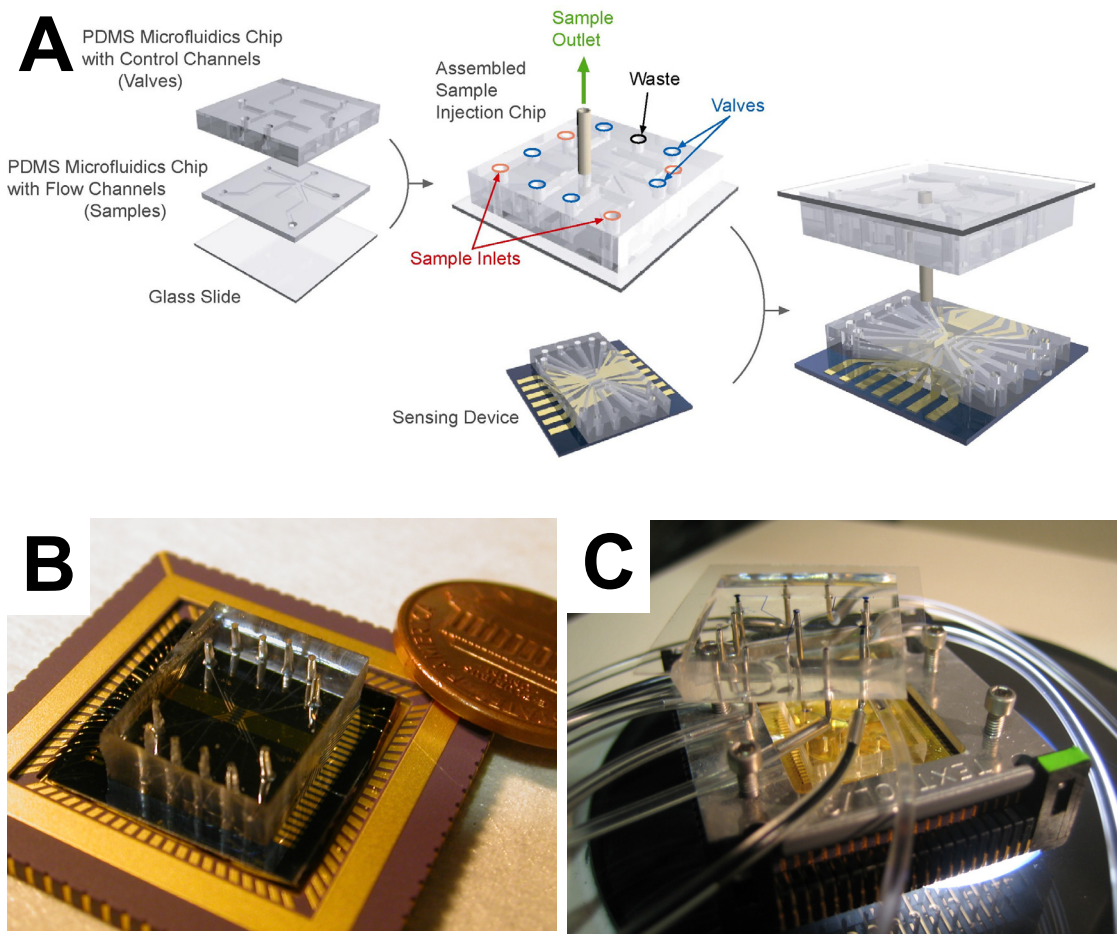

Figure 3.2: A) Fabrication and assembly of the two-layer PDMS chip for solution injection (top) with the sensing device composed of SOI wafer and a single-layer PDMS chip with six separate microchannels (bottom). B) A photograph of a sensing device with PDMS chip containing six microchannels. The chip is fixed onto a chip carrier and the gold pads on the device are wirebonded to the gold pads of the chip carrier. C) The sensing device with the PDMS chip on a chip carrier (B) is fixed into a chip carrier socket, and the PDMS chip for solution injection (A, top) is shown connected to one of the six microchannels of the sensing device, as outlined in the schematic A. The tubing with different solutions is feeding into the solution injection chip.

To automate an injection/changing of analyte solutions, we also introduced a second PDMS chip which can sequentially inject four different solutions into one of six

microchannels on silicon wafer. Such sample injection chip is composed of two layers, control layer and flow layer (Figure 3.2A). For the fabrication of the flow layer, mixed PDMS was spin coated on a photoresist mold at 2500 rpm for 50 sec and incompletely cured at 80 ^{o}C for 30 minutes. Control layer was fabricated by applying mixed PDMS over a photoresist mold directly and incompletely curing at 80 ^{o}C, followed by the puncturing of holes for inlets and outlets. The two layers were aligned together and the inlets/outlets for the flow layer were created. After two hours at 80 ^{o}C, the two-layer PDMS chip was bonded to a glass slide via an O_2 plasma treatment. By utilizing such sample injection chip, we were able to control the injection and solution-changing processes without disturbing the measurement, while maintaining the sensing device in an electrically isolated chamber at all times. The valves of the sample injection chip were actuated with the Labview program by means of the BOB3 Microfluidic Valve Manifold Controller and solenoid cluster manifolds (Fluidigm, San Francisco, CA). By introducing a waste outlet into the sample injection chip, we were able to remove any bubbles arising from switching between different solutions, which also helped in maintaining a stable baseline reading.

3.2.2 Surface Functionalization and Characterization

Synthesis *of tert*-Butyl allylcarbamate. To a solution of allylamine (2.27 g, 39.8 mmol) in THF (20 mL) was added *N,N*-diisopropylethylamine (13 mL, 80.0 mmol) followed by di-*tert*-butyl dicarbonate (8.7 g, 39.9 mmol). After 1 hr, the organic solvent was evaporated under reduced pressure, and the residue was purified by silica gel chromatography (Hex:EtOAc = 9:1) to give 6.6 g (93%) of a product as a clear oil. ^{1}H NMR 300 MHz ($CDCl_3$) δ 5.82 (m, 1H), 5.12 (m, 2H), 3.74 (bm, 2H), 1.45 (s, 9H).

Surface functionalization. The two procedures used to functionalize SiNWs with and without oxide layer are shown in Schemes 3.1 and 3.2, respectively.

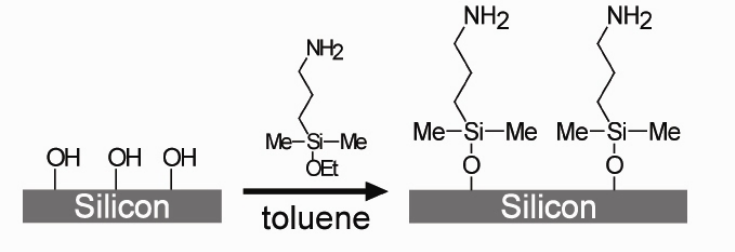

Scheme 3.1: Functionalization of Si(100) oxide surface with amine.

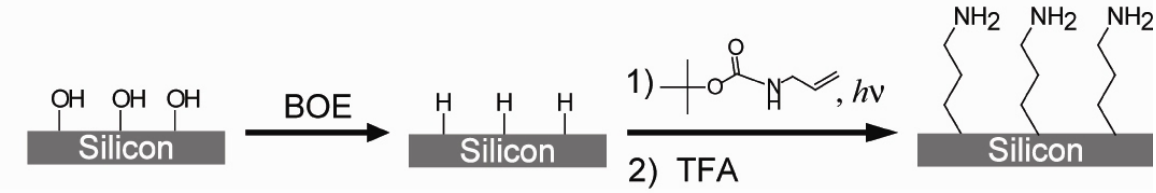

Scheme 3.2: Functionalization of Si(100) surface with amine.

Both procedures resulted in an amine terminated organic monolayer atop SiNWs. For the oxide surface functionalization, cleaned SiNWs were treated with 2% (v/v) 3-aminopropyldimethylethoxysilane (Gelest, Morrisville, PA) in toluene for 2 hrs. The wafers were then rinsed in toluene and methanol and incubated at 100 ^{o}C for 1 hr.

The procedure described previously[38, 44] (chapter 4) was used to functionalize hydrogen terminated SiNWs with *tert*-Butyl allylcarbamate (scheme 3.2). SiNWs were immersed in 2% HF solution for 3 seconds, washed with Millipore water and blow-dried under N_2 stream. The wafer was immediately placed in a custom made quartz container which was then pumped down to ~10^{-5} Torr, followed by an argon purge. Under positive argon pressure, a mixture of 1:2 *tert*-Butyl allylcarbamate:methanol (v/v) was applied to the wafer, completely covering the SiNWs. The wafer was illuminated with UV (254 nm, 9 mW/cm^2 at 10 cm) for 3 hours. SiNWs were then rinsed in methylene chloride and methanol. The deprotection of t-Boc amine was carried out in a solution of TFA in

methanol (1:4 v/v) for 4 hours, followed by extensive methanol washing. In the case of antibody attachment, the amine terminated surfaces were reacted with water-soluble homobifunctional N-hydroxysuccinimide ester (NHS ester), followed by the introduction of 50 mg/ml of monoclonal anti human IL-2 or anti human TNFα antibodies. The unreacted amines were quenched with ethanolamine (100mM in 1×PBS).

X-ray photoelectron spectroscopy. X-ray photoelectron spectroscopy (XPS) was utilized to quantify the amount of oxide on Si(100) wafers after surface treatments outlined in Schemes 3.1 and 3.2. XPS was also used to follow the attachment of antibodies to silicon surfaces. All XPS measurements were performed in an ultrahigh vacuum chamber of an M-probe surface spectrometer that has been previously described.[49] Experiments were performed at room temperature, with 1486.6 eV X-ray from the Al Kα line and a 35^{o} incident angle measured from the sample surface. ESCA-2000 software was used to collect the data. An approach described elsewhere[36, 49] was used to fit the Si 2p peaks and quantify the amount of surface SiO_x, assuming that the oxide layer was very thin. Any peak between 100 eV and 104 eV was assigned to Si^{+}-Si^{4+} and fitted as described in the literature.[50] SiO_x:Si 2p peak ratio was divided by a normalization constant of 0.17 for Si(100) surfaces.

Contact angle measurements. The sessile contact angle of water on the functionalized Si(100) surface was used to check the fidelity of surface chemistry as described in Schemes 3.1 and 3.2. Contact angle measurements were obtained with an NRL C.A. Goniometer Model #100-00 (Rame-Hart, Netcong, NJ) at room temperature. All measurements were repeated three times and averaged to obtain the contact angle θ for the surface.

3.2.3 SPR and Electronic Measurements

Surface plasmon resonance (SPR). All SPR experiments were performed on the Biacore 3000 with carboxylic acid terminated Biacore CM5 chips. The active flow cells were first primed in 1x SSC (15 mM NaCitrate, 150 mM NaCl, pH 7.5). To generate an amine surface, the carboxylic acid groups were converted to succinimide esters by flowing EDC/NHS prior to exposure of a 1 mg/ml solution of polylysine (Sigma-Aldrich, St. Louis, MO). Single stranded DNA (5'TGGACGCATTGCACAT3', Midland Certified, Midland, TX) was electrostatically absorbed unto the polylysine matrix. Complementary DNA was then immediately introduced and allowed to hybridize to the active surface. The flow cell was regenerated with two 1 minute pulses of 50 mM NaOH, after which ssDNA was reabsorbed electrostatically before another cDNA pulse was introduced for hybridization. The antibodies in acetate buffer (pH 5.5) were attached directly immediately following the surface treatment with EDC/NHS, and the remaining esters were reacted with ethanolamine. The antigen was introduced at various concentrations in 1x PBS buffer at the flow rate of 30 μl/min. Between each addition, the surface was regenerated with glycine/HCl buffer (pH 3.0).

Electronic measurements. The 4-point resistivity of silicon film as well as SiNW resistances and solution gating were measured with Keithley 2400 Source Meter (Keithley Instruments, Cleveland, OH). The sensing experiments were performed with SR830 DSP lock-in Amplifier (Stanford Research Systems, Sunnyvale, CA). Figure 3.3 shows the experimental setup for the electronic measurements. A 50 mVrms at 13 Hz voltage source (V_{SD}) was applied to one terminal of the nanowire, with the amplifier input operating in the current-measure mode. For the DNA-sensing experiments,

platinum wire was inserted into the microchannel and used as a solution gate, while it was kept at a ground potential throughout the real-time measurements to

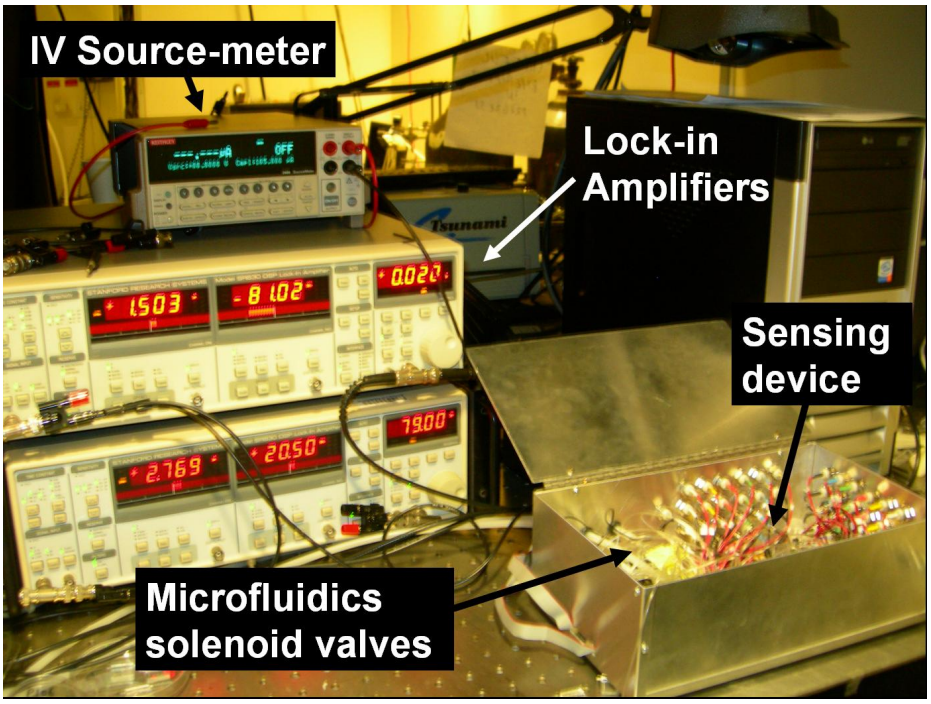

Figure 3.3: Experimental setup for biological sensing with silicon nanowires. The sensing devices (Figure 3.2C) are placed inside an electrically isolated box, which also contains solenoid manifolds that actuate microfluidic valves. The nanowire resistance is recorded in real time with lock-in amplifiers.

reduce the noise in the system (Figure 3.1A). In the case of protein sensing, the handle of the wafer (backside Si) was held at a ground potential instead of the platinum electrode in solution. The devices were functionalized and assembled as described above. Single stranded 10 μM DNA (same as in SPR experiments) in 1x SSC buffer was flowed through the microchannel for 1 hr and allowed to electrostatically adsorb to the amine terminated surface of SiNWs. The nonbound DNA was washed thoroughly with 1x SSC buffer. Complementary DNA (5'ATGTGCAATGCGTCCA3', Midland Certified, Midland, TX) of varying concentrations in 1x SSC buffer was sequentially injected from the injection PDMS chip into the microchannel containing SiNWs at a flow rate of 2.0

μl/min as the resistance of the NWs was recorded in real time. Noncomplementary DNA (noncomp. DNA) (5'CATGCATGATGTCACG3') was used as a control. In general, a different SiNW sensor was utilized for each of the measurements described here. Similar procedure was followed for protein sensing. The surface functionalized with capture antibodies was subjected to the 10 μM PBS solution containing various antigen concentrations (1 pM to 100 nM). After the introduction of a particular concentration, the surface was completely regenerated with 10 μM PBS, followed by the introduction of the next antigen concentration in the same microchannel.

3.3 Single-Stranded DNA Sensing

3.3.1 Nanowire Surface Passivation

We used contact angle measurements to follow the functionalization processes of various surfaces. Table 3.1 presents the data for both Schemes 3.1 and 3.2 (See Experimental Methods Section). The procedure in Scheme 3.1 generates a large increase in contact angle. Similarly, large changes in contact angles are observed for photochemically treated Si surface before and after t-Boc deprotection. The resulting contact angle of ~60^{o} is observed for surfaces prepared by Scheme 3.1 and 3.2, arguing for an existence of chemically similar, amine terminated monolayers on these surfaces.

Table 3.1: Measured contact angles for various Si(100) surfaces.

Si(100) surface	contact angle (deg)
With nonfunctionalized oxide	11 ± 1
Scheme 1: amine terminated	61 ± 1
Scheme 2: t-Boc protected	81 ± 1
Scheme 2: deprotected, amine terminated	60 ± 1

Quantifying the amount of oxide on the SOI NWs is extremely challenging. Therefore, we used Si(100) bulk surfaces to approximate the amount of surface oxide remaining after photochemical functionalization. Figure 3.4A shows XPS scan in the Si/SiO_x region. The Si(100) surface with native oxide exhibited approximately 1.9 equivalent monolayers of SiO_x. In contrast, the Si(100) surface treated according to Scheme 3.2 contained 0.08 equivalent monolayers of SiO_x prior to TFA deprotection and 0.3 monolayers of SiO_x after the deprotection step and a 10 hr exposure to 1x SSC buffer.

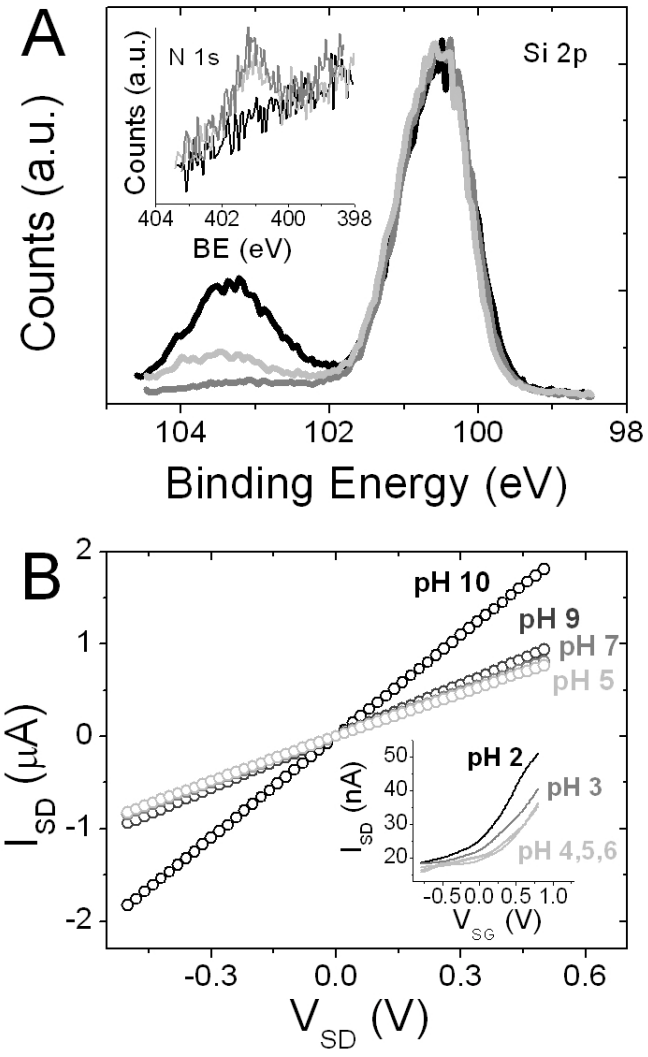

Figure 3.4: A) XPS of Si 2p region of Si(100) surface functionalized as in Scheme 3.2 before (dark grey) and after (light grey) TFA deprotection and 10 hr in 1x SSC buffer. Nonfunctionalized Si(100) surface with native oxide (black). Inset: N 1s region of nonfunctionalized Si(100) surface (black), Si(100) functionalized by Scheme 3.1 (light grey) and Scheme 3.2 (dark grey). B) Current-Voltage (IV) graphs of SiNWs functionalized by Scheme 3.1 in solutions of varying pH. Inset: solution gated (V_{SG}) n-type hydroxyl terminated SiNW in solutions of varying pH.

The roughness of a SiNW surface may cause a more extensive oxidation than the one observed on the bulk surface, but the data in Figure 3.4A does demonstrate a significant reduction in oxide thickness after photochemical treatment. Furthermore, we used XPS to determine the presence of amine terminated monolayer on bulk Si(100) surfaces post functionalization with two different schemes. Figure 3.4A inset demonstrates the XPS scans of N 1s region. Nitrogen peak is clearly visible for surfaces functionalized by Schemes 3.1 and 3.2, while no peak is present for the nonfunctionalized Si.

Scheme 3.1 functionalized SiNWs demonstrate sensitivity to pH which is different than for native oxide-passivated NWs.[13] The isoelectric point of silica is ~2,[51] implying that for hydroxyl terminated, non-functionalized SiNWs at low pH, the SiOH groups are largely protonated. At high pH, negative charges on SiO^- should deplete carriers in the n-type SiNWs, causing a decrease in I_{DS} (Figure 3.4B, inset). Above pH 4 the conductance is no longer modulated by increasing the pH, as most of the hydroxyl groups are deprotonated. When the surface is functionalized with amine ($pK_a \approx 9$-10), the opposite trend is expected. At low pH, the amine is protonated, causing carrier depletion or increased resistance in p-type SiNW. This trend is observed in Figure 3.4B, where the sharpest transition in resistance occurs between pH 9 and 10. The observation of the correct pH effects on the resistance of the SiNWs serves as a confirmation of the presence of surface functional groups, amine in this case.

As shown in Figure 3.5, oxide covered SiNWs (~8e18 cm^{-3} doping level) in 1x SSC buffer (0.165M, pH 7.2) respond weakly to the applied solution gate voltage, V_{SG}, showing no significant on-off current transition between 0.8 and -0.8 Volts.

In contrast, directly passivated SiNWs (Scheme 3.2) exhibit on-off current rations of ~10^2. Figure 3.5 strongly suggests that directly passivated SiNWs exhibit an enhanced response to surface charges and should therefore serve as superior NW sensors compared with similarly functionalized, but oxide-passivated SiNWs.

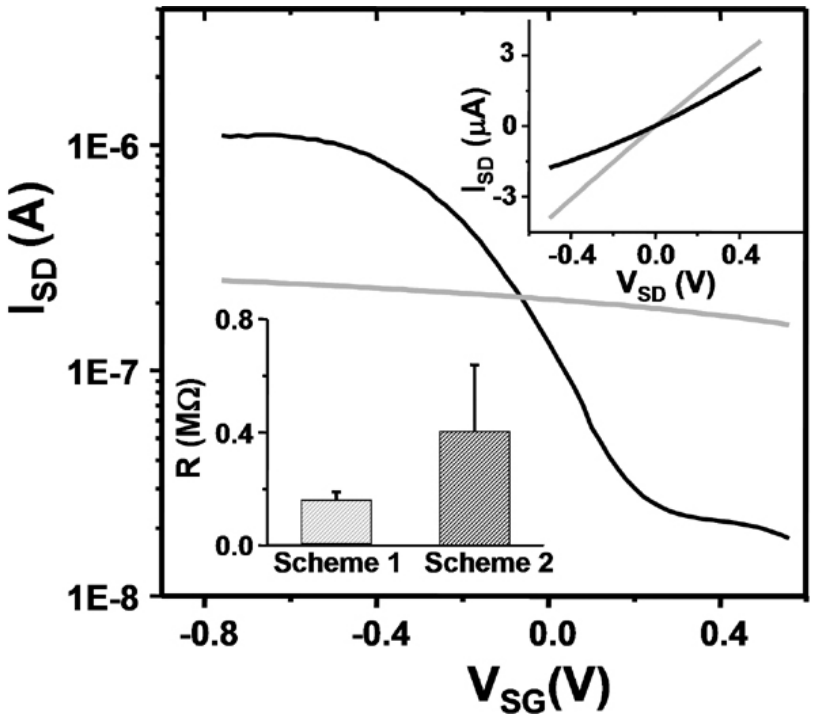

Figure 3.5: Solution gating of SiNWs functionalized by Scheme 3.1 (grey) and by Scheme 3.2 (black) (V_{SD} was 50 mV). (Right inset) IV curves of SiNWs in air with (black) and without (grey) oxide. (Left inset) Resistances in air of SiNWs functionalized by Scheme 3.1 (left) and Scheme 3.2 (right).

The Scheme 3.2 procedure does involve an HF etch step, which can be potentially detrimental to the device conductance. We, therefore, checked the conductivity of SiNWs before and after photochemical treatment. Lightly doped SiNWs provide for superior FET properties,[52] and, in fact, we have reported that lightly doped (10^{17} cm^{-3}) p- or n-type SiNWs are more sensitive biomolecular sensors than the highly doped nanowires (10^{19} cm^{-3}) (section 3.3.2).[53] Our doping process preferentially dopes the top few nanometers of the SiNWs, as described in chapter 2.[54] Thus, if the HF etching of the

Si surface was extensive enough, we could expect an enhancement in SiNW current modulation by V_{SG} to be entirely due to the decrease in carrier concentration and not the removal of surface oxide. The insets in Figure 3.5 demonstrate that the NW resistance increased only, on average, by a factor of 2 following the HF treatment. This relatively

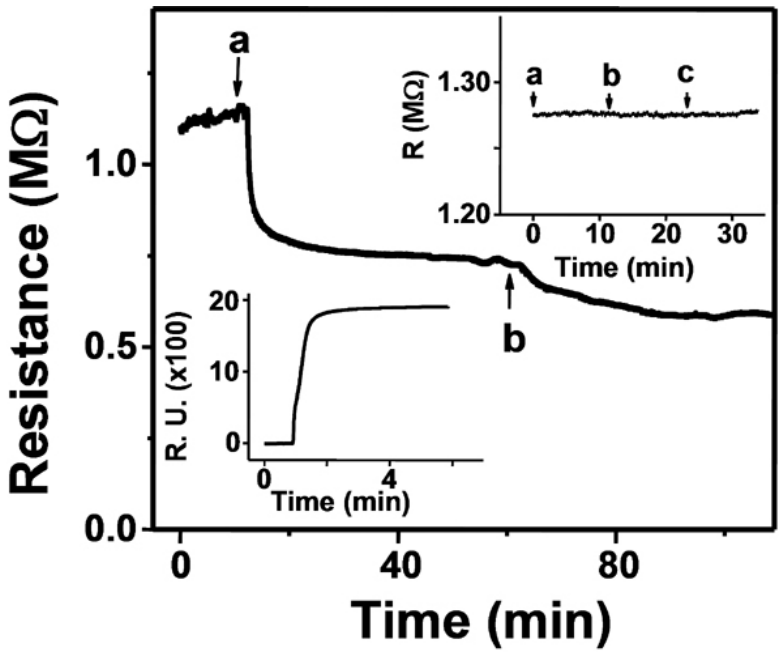

Figure 3.6: Real-time response of SiNWs functionalized as in Scheme 3.1 to the addition of (a) 10μM ssDNA and (b) 100nM complementary DNA. Right top inset: Real-time SiNW response to the sequential addition of (a) 0.165M SSC, (b) 0.0165M SSC, and (c) 0.00165M SSC buffers. Left inset: SPR measurement demonstrating the addition of 10μM ssDNA to poly-L-lysine coated CM5 sensor chip. V_{SD} = 50mV.

negligible resistance increase indicates that the major reason that the SiNWs prepared by Scheme 3.2 exhibit an improved solution FET performance originates from the elimination of oxide via direct silicon passivation. This result is consistent with the recent demonstration that, for VLS grown SiNWs, direct methylation of the SiNW surface leads to a 10^3 to 10^4 fold enhancement in the on-off conductance of the FETs made from those nanowires.[39]

Figure 3.6 shows SiNW real-time detection of the electrostatic adsorption of 10μM single-stranded DNA (ssDNA), followed by the hybridization in 1x SSC buffer of 100nM complementary DNA strand. As expected, the resistance of p-type SiNWs is decreased with the addition of negative surface charges. The metal contacts to NWs have been covered with Si_3N_4 layer, and there is no background conductance through the solution. We have observed an insignificant change in the resistance of the highly doped NWs upon switching from dry environment to buffer solution (data not shown). Moreover, as Figure 3.6 (right inset) shows, changing the ionic strength of the solution does not affect the resistance. This behavior is particular to highly doped wires. The low doped wires do show a change in conductance as the ionic strength of the solution is varied. In addition, the automated solution injection (section 3.2.1) removes any baseline shifts or transient changes in the resistance. SPR was also utilized in parallel to SiNWs in order to validate the surface chemistry and to obtain kinetic parameters such as κ_{on}, κ_{off} and affinity constant K_A for this particular DNA pair. Poly-L-lysine was covalently attached to the SPR sensor chips, mimicking the amine terminated monolayer of SiNWs. Figure 3.6 (left inset) shows the SPR response to the electrostatic adsorption of primary DNA from a 10μM DNA solution. The surface density of adsorbed DNA was estimated as 2.5×10^{13} cm^{-2}, using the conversion factor of 1000RU = 100 ng cm^{-2} from the literature.[55] The surface density is approximately an order of magnitude higher than the average surface density of 10^{12} cm^{-2} obtained when localizing biotinylated DNA on a streptavidin covered surface.[56] Such high surface density of primary DNA is expected because the poly-L-lysine treated surface is positively charged. It is likely that the amine-terminated SiNW surface has less surface charges than the poly-L-lysine covered surface and thus contains fewer sites for electrostatic adsorption of oligonucleotides.

Figure 3.7 demonstrates real-time label free detection of ssDNA by SiNWs and by SPR. In either case, the primary DNA strand was electrostatically immobilized on the sensor surface. Known DNA concentrations were injected after a stable reading with 1x SSC buffer was obtained, and the flow was maintained throughout the experiment. Different concentrations were detected with different groups of SiNWs. We observed that the hybridization on SiNWs is essentially irreversible on the relevant time scales when the analyte DNA was being washed away with the buffer solution. Such behavior is in contrast to SPR measurements, where the slow reversal of hybridization was observed (Figure 3.7C). The performance of the NWs functionalized according to Scheme 3.1 (Figure 3.7A) was compared to SiNW sensors prepared according to Scheme 3.2 (Figure 3.7B). The SPR experiments, although carried out on Au substrates, also utilized primary ssDNA that was electrostatically adsorbed onto an amine terminated surface. The intention here was to find experimental conditions that could serve to validate the NW experiments by obtaining kinetic parameters for these particular DNA strands under specific experimental conditions. Control experiments with noncomplementary DNA yielded no response for either SiNWs or SPR measurements (black traces of Figures 3.7A and 3.7C). These negative controls were also independently validated via fluorescent detection in microfluidic channels on two different Si surfaces (Figures 3.7A and B, insets). Figure 3.7D demonstrates that the NW response ($\Delta R/R_o$) varies as log[DNA]. Such a logarithmic dependence has been previously reported.[21]

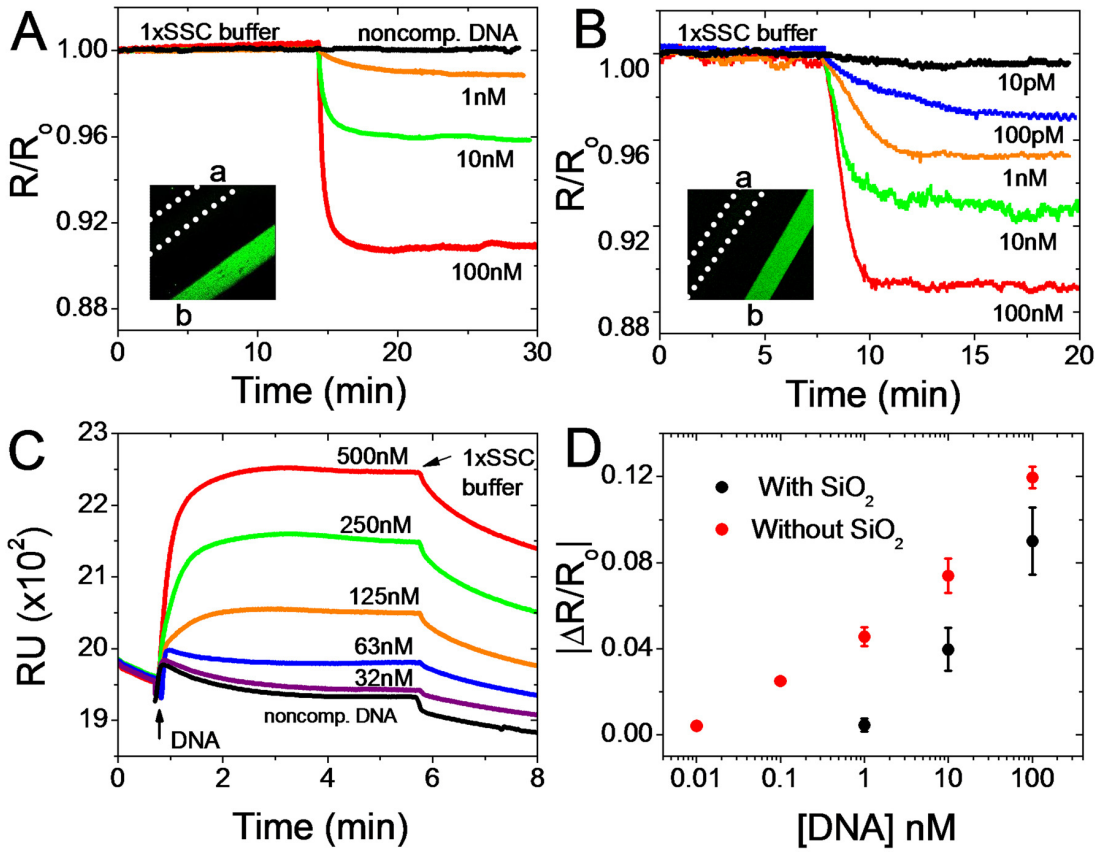

Figure 3.7: Concentration-dependent, real-time sensing of complementary DNA by SiNWs and by SPR in 0.165M electrolyte. A) Real-time responses of SiNWs that were surface functionalized according to Scheme 3.1 and coated with electrostatically adsorbed primary DNA. The black trace represents exposure of the SiNW sensors to 100nM non-complementary ssDNA. Each curve represents measurements from a different set of NWs. Inset: Fluorescence image of Si(100) surface (with overlaying PDMS microfluidics chip) treated as in Scheme 3.1 followed by 10μM primary DNA addition and addition of (microchannel a) 100nM noncomplementary fluorescent DNA and (microchannel b) 100nM complemenatary fluorescent DNA. PDMS chip was removed before the image was collected. B) As in A, except the SiNWs were functionalized according to Scheme 3.2. Inset: Same as in A inset, but Si(100) surface was treated as in Scheme 3.2. C) SPR measurement of the hybridization of complementary DNA to electrostatically adsorbed primary DNA on a poly-L-lysine surface. D) Normalized SiNW responses for Scheme 3.1 (black dots) and Scheme 3.2 (red dots) surface preparations, as a function of the log of DNA concentration. For all measurements, V_{SD} = 50mV.

As demonstrated in Figure 3.7D, the dynamic range of SiNWs is increased by 100 after the removal of oxide and UV-initiated chemical passivation; the limit of detection (LOD) increased from 1nM to 10pM.

3.3.2 Nanowire Impurity Doping Level

The way a semiconductor material such as silicon responds to surface potential or surface charges strongly depends on the impurity concentration (doping level) inside the material.[57] Highly doped devices exhibit short Debye lengths and short depletion regions. The Debye length, L_D, is inversely proportional to the square root of the impurity concentration, N.[57] L_D is a measure of how effectively the electric field is screened inside a material. Short L_D means that the screening is highly effective. For example, L_D of silicon doped at ~10^{17} is approximately 10 nm, and that of ~10^{19} doped silicon is only 1 nm.[57] Our silicon nanowires are doped non-uniformly: the top 10 nanometers of the wire are doped the heaviest, with the effective doping decreasing by an order of magnitude approximately 10 nanometers from the top surface of the wire. Therefore, we would expect that the nanowires doped at ~10^{17} will be the most sensitive to surface charge fluctuations due to molecular binding events in solution. Microscale EIS (electrolyte-insulator-silicon) FET devices were shown to be sensitive to the surface binding of DNA only when the sensor was doped at extremely low level of ~10^{15}.[58] The doping level is, therefore, an extremely important parameter to optimize, and, unlike the VLS grown wires, where the doping level is very hard to control precisely, SNAP method combined with SOD (spin-on doping, chapter 2) allows us to vary the doping of nanowires in a highly predictable and reproducible fashion.

In Figure 3.8A we present typical I-V curves for lightly doped p- and n-type SiNWs used for biological sensing. The linearity of the graphs suggests that the

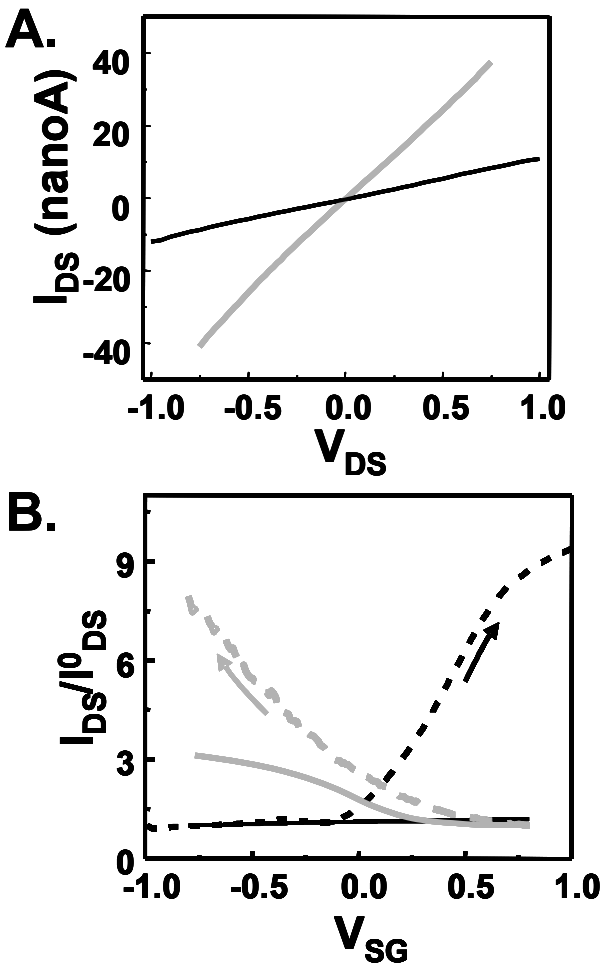

Figure 3.8: A) IV curves of p-type (grey) and n-type (black) SiNWs with dopant concentration of ~3e17 cm^{-3}. B) Solution gating (V_{SG}) of non-functionalized p-type (grey) and n-type (black) SiNWs with doping concentrations of: n-type ~3e17 cm^{-3} (dashed), ~1e19 cm^{-3} (solid); p-type ~3e17 cm^{-3} (dashed), ~3e18 cm^{-3} (solid). Arrows show the direction of the gate scan. I^{o}_{DS} is an initial current. V_{DS} was 50mV and electrolyte was 1× SSC buffer.

electrical contacts are ohmic. Moreover, the contact resistances are negligible compared with 10^{7} to 10^{8} Ω resistances of lightly doped SiNWs. Slight variations in measured resistances are expected due to a variable number of SiNWs contacted by the S/D contacts (between 5 and 10). We are currently working towards an individually

addressable arrays of SiNW sensors.[54] The resistance obtained from the slopes of I-V graphs may be used to estimate the doping concentrations, assuming mobilities of 100 cm^2/Vs and 300 cm^2/Vs for lightly doped (100) p-type and n-type silicon.[57] The resulting values of ~3.5e17 cm^{-3} for n-type and ~5.6e17 cm^{-3} for p-type agree well with the doping concentration of ~3e17 cm^{-3} measured by the 4-point method on the initial 300 Å SOI film.

The ability of SiNWs to sense charged species on their surfaces is directly linked to their performance as FETs in aqueous solution. Figure 8B demonstrates that the drain-source current (I_{DS}) can be gated by the voltages applied to the Pt electrode patterned near the sensor with the solution acting as the gate dielectric. The gating profiles are consistent with p and n-type FETs: I_{DS} of n-type (p-type) wires increases with the application of positive (negative) gate bias. Lightly doped SiNWs yield larger dI_{DS}/dV_{SG} values, suggesting that the lightly doped NWs should be more sensitive biosensors. The sensing response of SiNWs has largely been attributed to the modulation of the conductance of the 1D NWs through a change in surface charges (probably a combination of charges on biomolecules/solvating ions and exclusion of water/ions by the biomolecules).

We investigated how the sensitivity of SiNWs to single stranded DNA changes as the doping concentration is varied (Figure 3.9). As expected, lightly doped p- and n-type NWs showed increased levels of sensitivity: nanowires with impurity concentrations in the range of 10^{17} cm^{-3} exhibited the best performance. Wires doped at ~10^{19} cm^{-3} and higher exhibited no detectable response to complementary DNA below the concentration

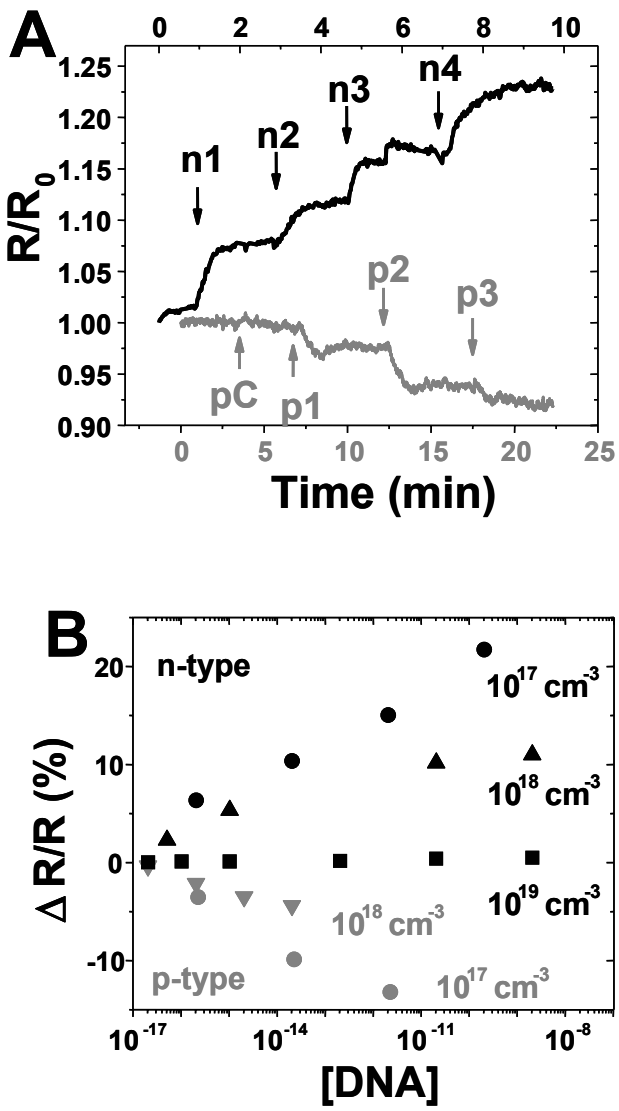

Figure 3.9: A) Real-time sensing results from n-type (black: top x-axis) and p-type (grey: bottom x-axis) SiNW sensors, both doped at ~ 3e17 cm^{-3}, demonstrating sensitivity in 100attoM (10^{-16}M) range in 1x SSC buffer. The various points indicated are (n-type) n1=220attoM, n2=22femtoM, n3=2.2pM, n4=220pM complementary DNA; (p-type) pC=22nM non-complementary DNA, p1=220attoM, p2= 22femtoM, p3=2.2pM complementary DNA. B) Both p- and n-type nanosensors exhibit sensitivity over a broad dynamic range. The sensitivities, however, depend on doping concentrations: n-type ~3e17 cm^{-3} (black circles), ~3e18 cm^{-3} (black triangles), ~1e19 cm^{-3} (black squares); p-type ~3e18 cm^{-3} (grey triangles), ~3e17 cm^{-3} (grey circles).

of 1nM, consistent with the data from Figure 3.7. The lower limit of detection of single-stranded 16-mer DNA for our NW sensors is at a concentration of approximately 1fM, consistent with other reported SiNW experiments.[14, 27] The dynamic range, defined as the range over which $\Delta R/R_0$ versus log[DNA] is linear, is approximately 10^6. As was mentioned previously, due to the electrostatic adsorption of primary DNA strand to the sensor surface, 1fM sensitivity is obtained in the high ionic strength (0.165M) solution. Therefore, proper engineering of the sensor, controlling impurity concentration and surface passivation, leads to optimized device performance. However, in the following section on protein sensing we will demonstrate that optimizing surface chemistry and the electronic properties of the sensor is not enough to obtain sensitivities which are significantly superior to optical detection. This is due to the fundamentally limiting effect of screening in high ionic strength solutions. In such environments, the size of the probe and the distance from the surface of the sensor at which the binding event takes place dominate the sensitivity of the electronic detection.

3.4 Protein Sensing

Robust label-free detection of proteins below the concentration of ~10pM is of considerable importance in rapid clinical evaluation, cancer marker detection, disease staging, etc. The real-time nature of electronic label-free detection also offers additional benefits such as characterization of new affinity probes, drug screening, and could, therefore, be potentially useful in basic research as well as in clinical practice. For these reasons, we have extended the above study to the detection of proteins. Such an endeavor, however, faces a fundamental challenge, owning to the significant charge screening in the solution of high ionic strength. The extent of such screening may be

characterized by the Debye length, $1/\kappa$,[20] which describes a distance from a point charge at which the potential due to that charge drops off to $\sim e^{-1}$ of its value. Scheme 3.3 demonstrates the relevance of Debye screening to the electrical detection of biomolecules in solution. Here, we assume that the antibodies, which serve as capture probes for proteins, are approximately 10 nm long, and are randomly oriented on the surface of the nanowire. The change in charge density, $\Delta\sigma$, due to the equilibrium binding of proteins is smeared over a distance b,

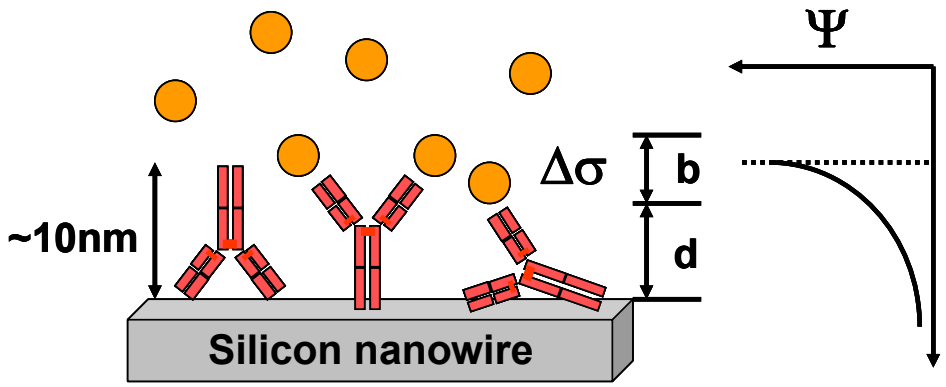

Scheme 3.3: The binding of proteins to antibodies at a distance ~10 nm from the surface of silicon nanowires results in an approximately homogeneous change in charge density, $\Delta\sigma$, which is smeared over a distance b. The accompanying change in chemical potential, Ψ, drops off exponentially, with a characteristic Debye length, $1/\kappa$.

which is a distance d away from the NW surface. The change in chemical potential per area at the surface of the nanowire may be described by the Debye-Hückel equation,[18, 20]

$$\Delta\Psi = \frac{\Delta\sigma}{b}\frac{\left[e^{-\kappa d} - e^{-\kappa(d+b)}\right]}{\varepsilon_0\varepsilon_w\kappa^2} \qquad (3.1)$$

where ε_0 is the dielectric constant, ε_w is the permittivity of water and κ^{-1} is the Debye screening length. As is readily noticeable from equation (3.1), the larger the $1/\kappa$ (smaller κ), the more pronounced will be the surface potential change for a given change in the

charge density. Surface potential and the distance from the surface at which the binding takes place are intimately coupled. If the screening length is much smaller than d, $\kappa^{-1} << d$, then the potential due to protein binding will be completely screened from the surface of the nanowire. Therefore, the condition $\kappa^{-1} \geq d$ must be met in order to detect charged species in the solution a distance d away from the surface. In the case of DNA sensing (section 3.3), the capture probe single-stranded DNA was electrostatically adsorbed on the NW surface, and the hybridization was taking place very close, ~1 nm from the surface, allowing us to carry out sensing in high ionic strength conditions of 0.165M. The antibodies, however, are fairly large biomolecules (Scheme 3.3). At 25 ^{o}C the Debye length of aqueous solution is[20]

$$\frac{1}{\kappa} = \frac{0.304}{\sqrt{[NaCl]}} nm \qquad (3.2)$$

for 1:1 electrolytes such as NaCl.

Table 3.2: Debye length at different salt concentrations

[NaCl]	**1/κ**
100mM	1nm
1mM	10nm
10μM	100nm

As Table 3.2 demonstrates, the size of the antibodies dictates the ionic strength of the solution in which the electronic detection may take place. This is a serious limitation if the physiological medium such as serium (0.14M) must be used to detect low abundance

proteins, without the possibility of appropriate dilutions. To circumvent this problem, new high-affinity probes such as aptamers, small molecules and short peptides must be developed, all of which are significantly smaller than the antibodies.

For protein sensing, devices were modified (original devices as in Figure 3.1) to include a control channel for each measurement (Figure 3.10), which contained

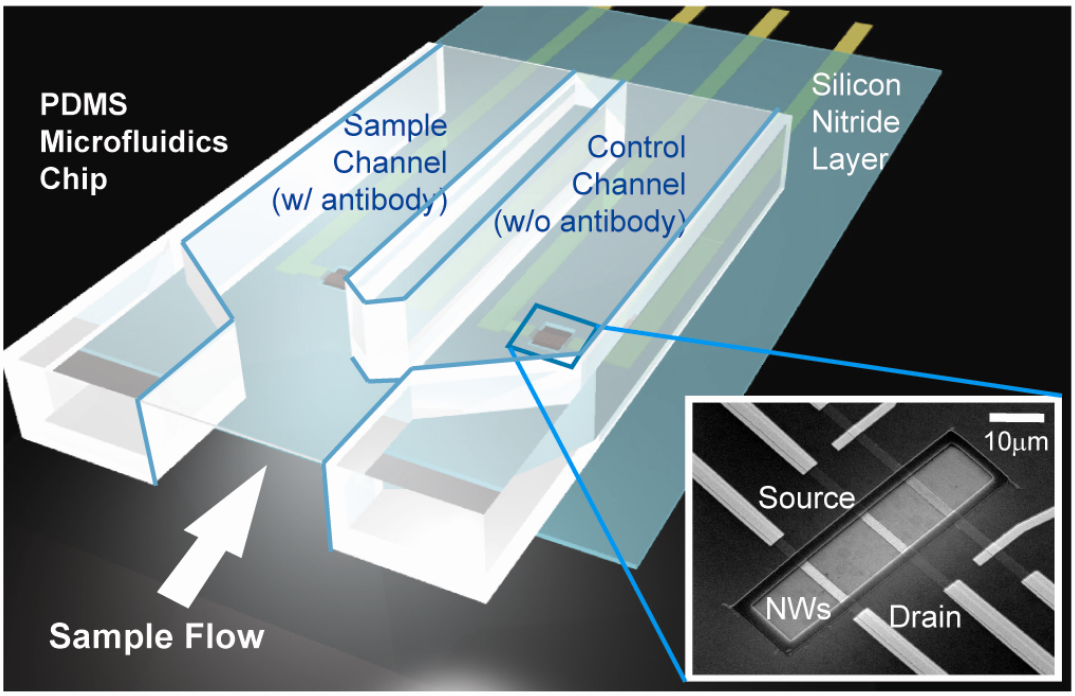

Figure 3.10: Schematic of the microfluidic PDMS chip overlaying a nanowire sensor device for differential measurements. A single microchannel bifurcates into two channels, each delivering solution to a separate sensor region with SiNWs (inset). One of the two sensor regions is functionalized with antibodies (left channel), while the other serves as a reference (right channel), accounting for the signal due to non-specific binding. The analyte solution is flown over both regions simultaneously (arrow), and the real-time resistance of the two regions is subtracted.

nonfunctionalized SiNWs. It is expected that such bare SiNWs provide a measure of nonspecific protein binding to the surface; therefore, a differential measurement taking biofouling and random drift into account is more accurate.

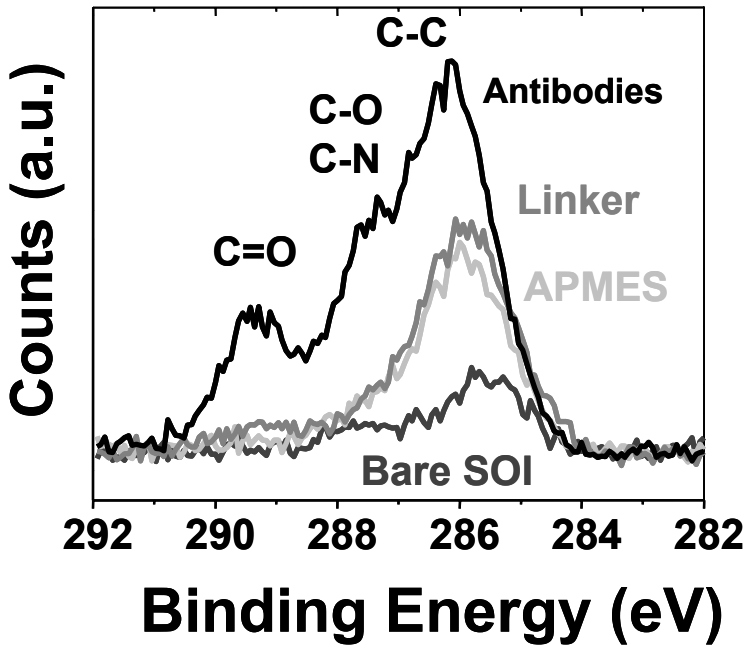

Figure 3.11: XPS of carbon 1s region, followed through the process of nanowire functionalization with antibodies. Starting with bare silicon-on-insulator (SOI) substrate (dark grey), the wafer is functionalized with 3-aminopropyldimethylethoxysilane (APMES) as described in experimental methods section (light grey). Bifunctional cross-linker (NHS ester) is then attached to the surface amines (grey), followed by the covalent attachment of antibodies (black).

SiNW surfaces for protein sensing were functionalized in a similar manner to the experiments with DNA. Native oxide of silicon was functionalized with amine-terminating monolayer. A bifunctional cross-linker, with an NHS ester on either end, was coupled to the primary amines on the surface, followed by the coupling of antibodies to the other end of the linker. This chemistry may potentially involve any of the primary amines of the antibody, and, therefore, probably results in a random orientation of the antibodies on the surface (Scheme 3.3). Since the surface area of a nanowire is rather small, $\sim 10^{-13}$ m^2, this may result in the broadening of the distribution of the responses from the identical nanowires. Measuring the response of a larger array of nanowires, therefore, may lead to a smaller variance in the response.

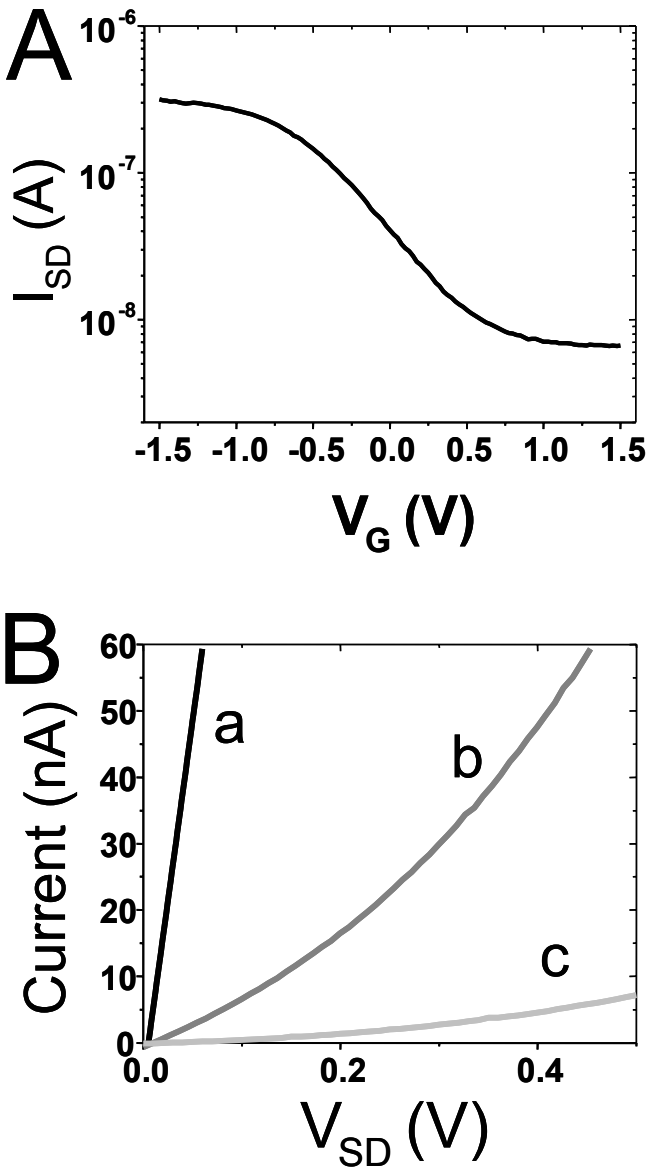

Figure 3.12: A) SiNW (~10^{18} cm^{-3}) response to the application of solution gate voltage in 10μM PBS solution. B) Current-voltage traces of SiNW (~10^{18} cm^{-3}) a) with surface amine in air, b) with surface amine in10μM PBS solution, c) after antibody attachment in 10μM PBS solution.

XPS scans of the carbon 1s region from the silicon surface treated as described above are presented in Figure 3.11. Clear emergence of the C=O and C-O/C-N bonds is visible, suggesting that the antibodies are successfully attached to the surface. Low doped nanowires (~10^{18} cm^{-3}) were used for this study based on the observation of the

influence of doping level on the sensitivity of SiNWs (Figure 3.9). This doping level was chosen as the one which reproducibly yields wires with resistances of ~1 MΩ, ohmic contacts and good solution transconductance behavior (Figure 3.12A). Wires with higher doping are not as sensitive to proteins and those with lower doping yield fewer functional devices.

The attachment of antibodies was further verified by monitoring the resistance of the nanowires during the functionalization process. Figure 3.12B shows IV curves of the nanowires in air, in solution, and after the attachment of the antibodies. The resistance of the amine-terminated nanowires drops significantly after immersion in solution and further yet after the attachment of the antibodies. The pH of the 10μM PBS is approximately 6.0, which may account for the increase in the resistance in the solution. It is also possible that pH 6.0 is below the isoelectric point of the particular antibody used here, and the excess positive charges on the antibody surface lead to the further increase in the resistance.

Real-time detection of proteins with SiNWs is demonstrated in Figures 3.13 and 3.14. In each case, the same microchannel (the same SiNWs) was used for introducing antigen at various concentrations. After the saturation of the signal, phosphate buffer was used to remove bound interleukin-2 (IL2). This process was repeated several times with different IL2 concentrations, and as Figures 3.13A and 3.14 demonstrate, the antigen-antibody binding is fully reversible. SiNWs can, therefore, similarly to the SPR chip, be reused multiple times for protein detection. The data in Figure 3.13 was collected in

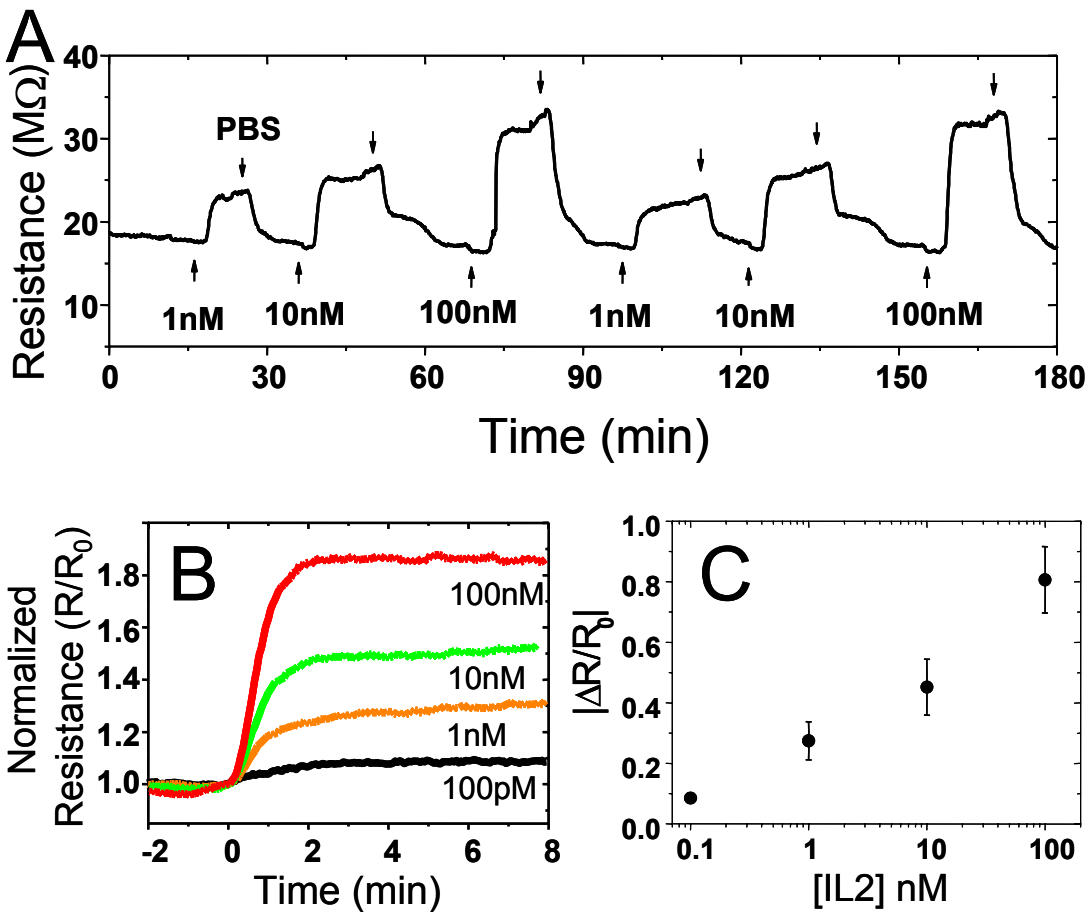

Figure 3.13: A) Real-time sensing of human IL2 with SiNWs doped at 10^{-18} cm^{-3}. The nanowires were functionalized with 3-aminopropyltriethoxysilane (APTES), followed by the attachment of anti human IL2 antibodies. Human IL2 in 1.5μM PBS at different concentrations (1nM, 10nM and 100nM) was introduced, each time followed by the removal of bound IL2 with 1.5μM PBS. B) Normalized resistance of nanowires (R_0 is an initial resistance) as a function of time and IL2 concentration. C) Normalized change in resistance $\{\Delta R/R_0=(R_{sat}-R_0)/R_0\}$ as a function of protein concentration.

1.5μM PBS using the chip which was functionalized with 3-aminopropyltriethoxysilane (APTES). APTES forms multilayers on the surface due to intermolecular polymerization. After the data in Figure 3.13 was collected, the chip was cleaned in organic solvents and briefly in O_2 plasma. The surface of SiNWs was then functionalized with 3-aminopropyldimethylethoxysilane (APMES), which forms a monolayer on silicon oxide surface. Subsequent protein sensing was carried out in 10μM PBS. As evident from

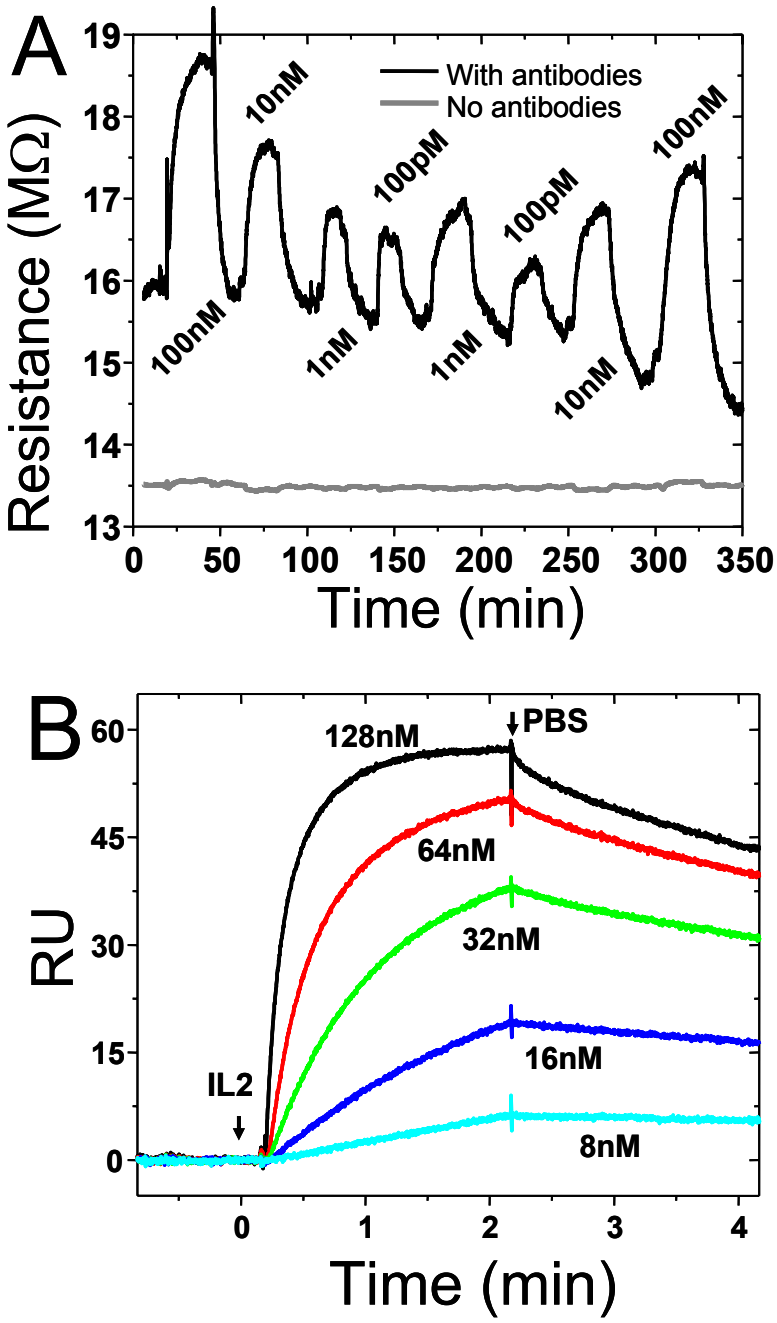

Figure 3.14: A) Real-time, differential sensing of human IL2 in 10μM PBS. The solutions containing IL2 at different concentrations (100nM, 10nM, 1nM and 100pM) were flown sequentially over an active region of SiNWs which were functionalized with antihuman IL2 antibodies (black curve), with the addition of 10mM PBS after each IL2 concentration to wash away bound proteins. Simultaneously, the same solutions were also introduced into a separate channel (Figure 3.10) containing SiNWs without antibodies on the surface (grey curve). B) SPR of IL2-antiIL2 antibody interaction at different concentrations of IL2. The flow rate was 30μl/min.

comparing Figures 3.13 and 3.14, while the same device was used for protein sensing, the changes in resistance corresponding to the same concentrations of IL2 are markedly different. The reason for this difference is difficult to pinpoint exactly. In Figure 3.13, the functionalization with APTES may have resulted in a higher density of surface

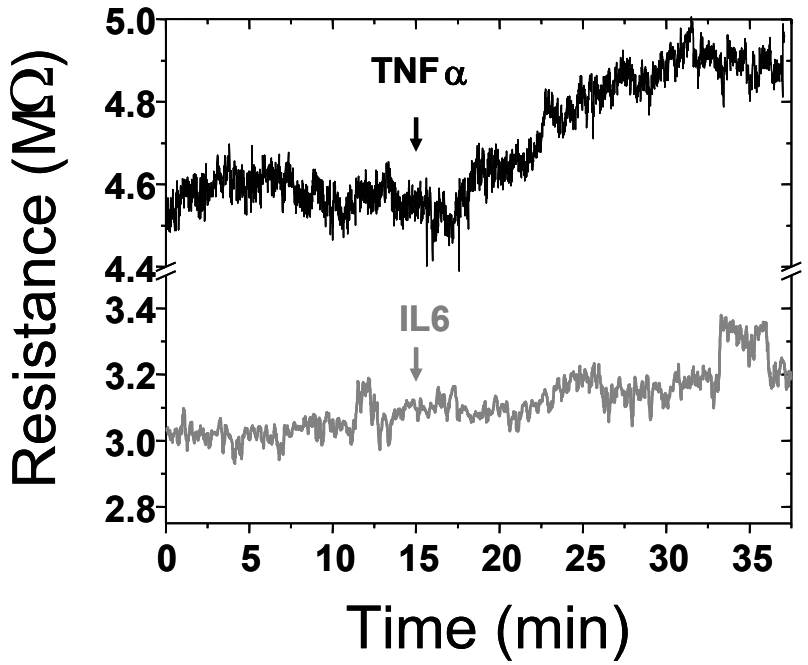

Figure 3.15: Real-time detection of 10nM TNFα with n-type 20 nm SiNWs (~10^{18} cm^{-3}) (black curve) functionalized with antiTNFα antibodies. Grey curve is the control experiment demonstrating no change in resistance upon introduction of 10nM IL6.

amines, which translated to a higher surface density of anti-IL2 antibodies, and, therefore, to a larger saturation signal. Also, longer Debye screening length, corresponding to the detection in 1.5μM PBS (Figure 3.13), versus 10μM PBS (Figure 3.14), may have also contributed to higher signals. Finally, O_2 treatment may have oxidized the surface, leading to a drop in sensitivity (chapter 4). Regardless of the exact reason, it is evident that the sensing devices may be reused multiple times for protein detection. Figure 3.14 demonstrates that the increase in resistance is specific to antibody-

IL2 binding. When the antibodies are absent from the SiNW surface, no changes in the resistance are observed, meaning that the nonspecific binding of the antigen is below the detection threshold. In addition, the response of the nanowires to the binding of IL2 is consistent with the majority surface charge of the protein. The isoelectric point of recombinant human IL-2 is between pH 6.5 and 7.5. Therefore in dilute PBS, pH ~6.0, there should be a prevalence of positive surface charges on the protein, leading to an increase in resistance of p-type silicon nanowires (Figures 3.13 and 3.14). In contrast, tumor necrosis factor alpha (TNFα) cytokine, with the isoelectric point of between pH 4 and 5, should have majority negative charges at pH 6.0. Figure 3.15 demonstrates the detection of TNFα with n-type SiNWs, which exhibit an increase in resistance, consistent with the lower isoelectric point of the cytokine.

The above protein sensing experiments demonstrate that it is possible to engineer silicon nanowires to detect protein concentrations below the detection limit of other label-free methods, such as SPR (Figure 3.14B). The detection of two important proteins, IL2 and TNFα, which are crucial cytokines of the immune system, is demonstrated. Potentially, this method may be utilized to detect low levels of cancer markers in the serum. For those applications especially, quantitative information about the fluctuation of protein concentrations in blood is of utmost importance. As shown above, a relative change in resistance of SiNWs for a given concentration of a protein may differ from device to device. The real-time and label-free nature of this method, however, affords a powerful opportunity to obtain quantitative kinetic information about protein-antibody interaction, and ultimately to convert that information into an absolute

protein concentration. In the next section, we will discuss a method of obtaining kinetic parameters from the kind of sensing data presented here.

3.5 Quantitative Analysis of Nanowire Response

3.5.1 Analysis of DNA-Sensing Experiments

SiNW sensors can potentially be utilized to quantitate analyte concentration and binding constants. In order to explore this possibility, the SiNW sensing response must be compared with other label-free, real-time methods such as SPR. It is also critical to design experimental parameters for both sensing modalities that are as similar as possible, as was described above. In this section, we first discuss the use of electrostatically adsorbed primary DNA for detecting complementary DNA analyte. We then discuss the development of a self-consistent model that allows for the direct comparison of SPR measurements with nanowire sensing data. Finally, we test that model by utilizing the nanowire sensing data to calculate 16-mer DNA binding constants and analyte concentrations.

Previous studies have demonstrated that the Langmuir model can be applied for parameterization of the hybridization processes of short oligonucleotides.[22, 56] We used the Langmuir model to calculate kinetic parameters from the SPR hybridization measurements (Figure 3.7C) and obtained $k_{on}=1\times10^{5}$, $k_{off}=2\times10^{-2}$, $K_A=5\times10^{6}$ (Table 3.3). This K_A value is between 10 and 100 times smaller than that reported for similar length DNA measured with a quartz crystal microbalance, SPR,[22] and surface plasmon diffraction sensors (SPDS).[56] The average primary DNA surface coverage in those studies was ~5×10^{12} molecules/cm^2. As stated above, the electrostatically adsorbed DNA

coverage in our SPR experiments was approximately 10 times higher, at 2.5×10^{13} cm^{-2}. This difference in coverage likely arises from the differing methods of DNA immobilization; while in our system the DNA is electrostatically adsorbed, other studies utilized a streptavidin-biotinylated DNA linkage for surface immobilization.[22, 56] High surface coverage of primary DNA significantly reduces the efficiency of hybridization.[56, 59] In addition, the hybridized duplex of electrostatically adsorbed and covalently bound DNA may be structurally and energetically different. It has been proposed that a preferred structural isomer of an oligonucleotide pair on a positively charged surface is a highly asymmetrical and unwound duplex.[60] We believe that such non-helical nature of DNA duplex, together with steric effects of highly packed surface play major roles in the reduced affinity for the 16-mer pair used in this study.

We now turn toward developing a model for using SiNW sensors to quantitate complementary DNA pair binding constants, and, if those numbers are known, to determine the solution concentration of the analyte. A discussion of the kinetics of a surface binding assay, as measured within flowing microfluidics environments, is required. Zimmermann and co-workers modeled the kinetics of surface immunoassays in microfluidics environments.[61] Their model was based on four differential equations: the two Navier-Stokes partial differential equations, the Convection-Diffusion equation, and the ordinary differential equation resulting from the Langmuir binding model (i.e., the binding/hybridization equilibrium). A key result was that in the limit of high analyte flow speeds (>0.5 mm/sec) (which is the case for all the experiments in this work) the process is reaction limited. Therefore, the amount of analyte that is captured and detected can be described by the ordinary differential equation resulting from the Langmuir binding model:

$$\frac{d\Theta_t}{dt} = k_{on}C\left(\Theta_{\max} - \Theta_t\right) - k_{off}\Theta_t \qquad (3.3)$$

Here, Θ_t=surface density of bound analyte molecules; κ_{on}=rate constant for association; κ_{off}=rate constant for dissociation; C=solution concentration of analyte (a constant under flowing conditions); Θ_{max}=maximum number of binding sites available per surface area. Equation (3.3) can be solved analytically to yield:

$$\Theta_t = \frac{k_{on}\Theta_{\max}C}{k_{on}C + k_{off}}\left(1 - e^{-\left(k_{on}C + k_{off}\right)t}\right) \qquad (3.4)$$

The challenge is to translate from the resistance change of a SiNW sensor to the analyte concentration, C. However, the exact relationship between a measured resistance change and the surface density of bound analyte molecules is not intuitively clear. Here we attempt to determine the nature of that relationship. We demonstrated above (Figure 3.7D) that the cumulative change in SiNW sensor resistance arising from the binding of a charged analyte (ssDNA) at a concentration-dependent saturation was linearly proportional to the log[DNA], similar to what has been reported for VLS SiNW detection of prostate specific antigen (PSA).[21] In mathematical terms, this means that as we approach saturation for a given concentration:

$$\frac{\Delta R}{R_0} = \alpha \ln C \qquad (3.5)$$

where α is a constant, $\Delta R = R - R_0$, R is resistance at time t, and R_0 is the resistance at t=0. At saturation levels equation (3.4) reduces to $\Theta_t = \frac{k_{on}\Theta_{\max}C}{k_{on}C + k_{off}} = \frac{K_A\Theta_{\max}C}{K_AC + 1}$ (where the

binding affinity $K_A = \frac{k_{on}}{k_{off}}$). In the limit where $K_A C << 1$ (which is usually the case

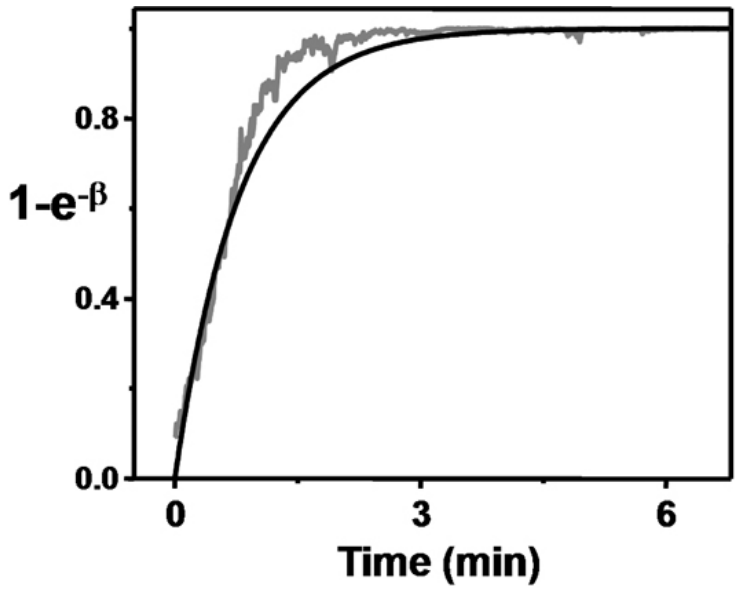

Figure 3.16: Comparison of SPR-derived hybridization kinetic parameters with NW sensing data. The black line represents equation (3.7) plotted using k_{on} and k_{off} obtained from SPR measurements, $\beta=(k_{on}C+k_{off})t$. The grey trace is obtained from SiNW resistance versus time data, $\beta = \frac{\Delta R}{R_{\max} - R}$. C = 10nM.

with values of C $\leq 10^{-9}$ and values of $K_A < 10^8$), this reduces to $\Theta_t = K_A \Theta_{\max} C$. Therefore, at saturation, and with $K_A C << 1$, Θ_t scales linearly with C. From our previous discussion, this implies that at saturation $\frac{\Delta R}{R_0}$ scales logarithmically with Θ_t (or equivalently that Θ_t is an exponential function of $\frac{\Delta R}{R_0}$ at saturation). In estimating the relationship between resistance changes at all times (not just at saturation) and the surface density of bound analyte molecules at all corresponding times, we start by assuming the same functional relationship that we experimentally observe at saturation. We also impose two boundary conditions: (1) when the measured resistance reaches its

saturation level we would expect the maximum number of binding events to have taken place and for that number to be consistent with the prediction from the Langmuir binding model (equation 3.4), and (2) when the measured resistance is unchanged from its starting level we expect zero binding events (again consistent with the Langmuir model at time=0). Based on these assumptions and boundary conditions we can thus estimate that the surface density of bound analyte molecules as a function of resistance change has the form:

$$\Theta_t = \frac{k_{on}\Theta_{\max}C}{k_{on}C + k_{off}}\left(1 - e^{\frac{-\Delta R}{R_{\max} - R}}\right) \qquad (R_{max}=R \text{ at saturation}) \qquad (3.6)$$

It is important to note that eq. (3.6) is only a guess based on the relationship observed experimentally. In the next section, we will attempt to derive a relationship which is consistent with the fundamentals of solid state physics. The validity of eq. (3.6) can be tested by considering the following expression that is derived from eq. (3.6) and comparing it to the same expression derived from eq. (3.4):

$$\Theta_t \Big/ \frac{k_{on}\Theta_{\max}C}{k_{on}C + k_{off}} = [1 - e^{\frac{-\Delta R}{R_{\max} - R}}] = [1 - e^{-(k_{on}C + k_{off})t}] \qquad (3.7)$$

Note that eq. (3.7) is expressing the fraction of bound analyte molecules at time t relative to the level at saturation in terms of ΔR (first term in brackets) and in terms of binding constants (second term in brackets). Time appears explicitly in the second term in brackets, while it is implicit in the first term in brackets (i.e., at a given time t there is a given *R* and ΔR). If we plot the first term in brackets in eq. (3.7) (the term containing

ΔR) against the second term in brackets (using κ_{on} and κ_{off} values from an SPR analysis), we find that the two curves are qualitatively similar (Figure 3.16).

A second test of eq. (3.6) is to utilize it to extract binding kinetics. As we can infer from eq. (3.7), if eq. (3.6) is equivalent to the Langmuir binding model (eq. 3.4), then:

$$\frac{\Delta R}{R_{\max} - R} = \left(k_{on} C + k_{off}\right) \times t \qquad (3.8)$$

We can thus extract κ_{on} and κ_{off} values from measured resistance data.

	SiNWs - concentration pair:			**SPR (this work) (poly-L-lysine surface, 16-mer DNA)**	**SPDS (ref. 56) (avidin-biotin linkage, 15-mer DNA)**
	10 nM 100 nM	1 nM 100 nM	1 nM 10 nM		
κ_{on} ($M^{-1} s^{-1}$)	3.5(3.4) × 10^5	4.2(2.4) × 10^5	6.2(9.6) × 10^5	1.01 × 10^5	6.58 × 10^4
κ_{off} (s^{-1})	3.1 (0.5) × 10^{-2}	2.4 (0.8) × 10^{-2}	2.4 (0.9) × 10^{-2}	2.01 × 10^{-2}	1.32 × 10^{-4}
K_A (M^{-1})	1.1 × 10^7	1.8 × 10^7	2.6 × 10^7	5.02 × 10^6	4.98 × 10^8
[DNA]	100 nM (actual); 68(52) nM calculated 10 nM (actual); 14(9) nM calculated				

Table 3.3: Kinetic Parameters estimated from SiNW biosensors for the hybridization of 16-mer DNA and corresponding comparisons with analogous SPR and SPDS (surface plasmon diffraction sensor).[56] The calculated concentrations (bottom row) were estimated with eq. (3.6), by using the pair of SiNW measurements that did not include the concentration to be determined. For example, the 1nM and 100nM measurements were used to determine the concentration at 10nM. Standard deviations are given in parentheses.

To extract κ_{on} and κ_{off} values from the resistance versus time data, we used eq. (3.8) to create a series of two equations with two unknowns (one equation from each concentration) which we solved to get the implied κ_{on} and κ_{off}. For each concentration in

the pair, we chose to use all data points starting at a time where our model (the first term in brackets in eq. 3.7) indicated a value of 0.63 (i.e., a time equal to the characteristic time of this experimental function) and ending 150 seconds later (time close to saturation, i.e., a value of 1 for eq. 3.7). We chose this part of the data because the assumptions underlying the model indicate that values close to saturation are the ones where our model fits real data the best. For each concentration pair, therefore, we had 150 pairs of equations, each yielding a value for κ_{on} and κ_{off}. To extract the implied concentration values from the resistance versus time data, we used eq. (3.8), this time using κ_{on} and κ_{off} values obtained from a concentration pair that did not contain the concentration we were trying to estimate. Again, we chose 150 data points from the same portion of the graph used to extract κ_{on} and κ_{off} values. Each data point yielded one equation in one unknown, which we solved to get the implied concentrations. We then calculated the average implied concentration and the standard deviation for all 150 data points. The κ_{on}, κ_{off}, and K_A values, along with the analyte concentrations, are summarized in Table 3.3. The κ_{on} constants determined from the SiNW experiments are 3 to 5 times larger than κ_{on} obtained with SPR experiments. The nanowire-measured κ_{off} values, however, are consistently quite close to those measured with SPR. As stated above, the variation in κ_{on} values may be a reflection of steric affects that arise from the unusually high surface density of primary DNA adsorbed onto the poly-L-lysine surfaces that were used for the SPR experiments.[56, 59]

3.5.2 Analysis of IL2-Sensing Experiments

In the previous section, eq. (3.6) was proposed based on the observation of linear relationship between the log of analyte concentration and $\Delta R/R_0$, as well as the

appropriate boundary conditions. It was demonstrated that kinetic parameters and analyte concentrations which are quite close to those measured with SPR could be derived from eq. (3.8). Here, we attempt to ground the derivation of kinetic parameters and analyte concentrations, obtained from the silicon nanowire sensing data, on the fundamentals of solid state physics. We assume, as in section 3.5.1, that the sensing process is reaction limited due to a high flow rate of solution containing the analyte, and that the nanowire response must, therefore, be consistent with the solution (eq. 3.4) to an ordinary differential equation (3.3). Let us define Θ_{sat} as a number of analyte molecules captured at saturation on the surface of a sensor:

$$\Theta_{sat} = \frac{k_{on}\Theta_{\max}C}{k_{on}C + k_{off}} \tag{3.9}$$

Further, let Θ_f be a fraction of the saturation value of molecules captured at time t:

$$\Theta_f = \frac{\Theta_t}{\Theta_{sat}} = \left(1 - e^{-\left(k_{on}C + k_{off}\right)t}\right) \tag{3.10}$$

We now turn to some fundamental equations describing the electronic properties of semiconductors.[57] The resistivity (ρ) of p-type material may be described as follows:

$$\rho = \frac{1}{q\mu p} \tag{3.11}$$

where q is hole charge, μ is the mobility of holes and p is the density of holes, given by:

$$p = n_i e^{\frac{\left(E_i - E_F\right)}{kT}} \tag{3.12}$$

where n_i is intrinsic carrier concentration, E_i is the intrinsic energy, E_F is Fermi energy, k is Boltzmann constant and T is the temperature. The resistance is given by $R=\rho L/A=\rho G$, where L is the length of the material and A is the area of the cross section. E_i can be rewritten as $E_i=-qV_G=-qA\Theta_t S$, where V_G is gate voltage, S is total charge on a bound analyte molecule and A is some proportionality constant relating chemical potential and total surface charge (similar to equation 3.1). Rewriting the expression for resistance R by combining equations (3.11) and (3.12), we obtain (G=L/A):

$$R = \frac{G}{q\mu n_i e^{-E_f/kT} e^{-qA\Theta_t S}} \tag{3.13}$$

Solving for Θ_t as a function of R yields:

$$\Theta_t = \frac{1}{qAS}\left[\ln\left(\frac{q\mu n_i}{Ge^{E_f/kT}}\right) + \ln(R)\right] \tag{3.14}$$

We invoke the boundary condition similar to those discussed in section 3.5.1. The number of captured molecules at saturation, when $R=R_{sat}$, equals Θ_{sat}.

$$\Theta_{sat} = \frac{1}{qAS}\left[\ln\left(\frac{q\mu n_i}{Ge^{E_f/kT}}\right) + \ln(R_{sat})\right] \tag{3.15}$$

At time zero (t=0) there are zero captured molecules ($\Theta_t=0$) and $R=R_0$.

$$0 = \frac{1}{qAS}\left[\ln\left(\frac{q\mu n_i}{Ge^{E_f/kT}}\right) + \ln(R_0)\right] \tag{3.16}$$

Therefore,

$$\ln\left(\frac{q\mu n_i}{Ge^{E_f/kT}}\right) = -\ln(R_0) \tag{3.17}$$

Finally, we can represent the fraction of molecules captures simply in terms of the nanowire resitance:

$$\Theta_f = \frac{\Theta_t}{\Theta_{sat}} = \frac{\frac{1}{qAS}\left(-\ln(R_0)+\ln(R)\right)}{\frac{1}{qAS}\left(-\ln(R_0)+\ln(R)\right)} = \frac{\ln\left(\frac{R}{R_0}\right)}{\ln\left(\frac{R_{sat}}{R_0}\right)} \tag{3.18}$$

Equations (3.10) (Langmuir model) and (3.18) (solid state physics) both represent the fraction of captured molecules and can be equated.

$$\Theta_f = \frac{\ln\left(\frac{R}{R_0}\right)}{\ln\left(\frac{R_{sat}}{R_0}\right)} = \left(1 - e^{-\left(\kappa_{on}C+\kappa_{off}\right)t}\right) \tag{3.19}$$

Therefore, if the kinetic parameters κ_{on} and κ_{off} are known, the concentration can be obtained from the resistance value at any time t.

$$C = -\frac{1}{\kappa_{on}t}\left(\ln\left(1 - \frac{\ln\left(\frac{R}{R_0}\right)}{\ln\left(\frac{R_{sat}}{R_0}\right)}\right) + \kappa_{off}t\right) \tag{3.20}$$

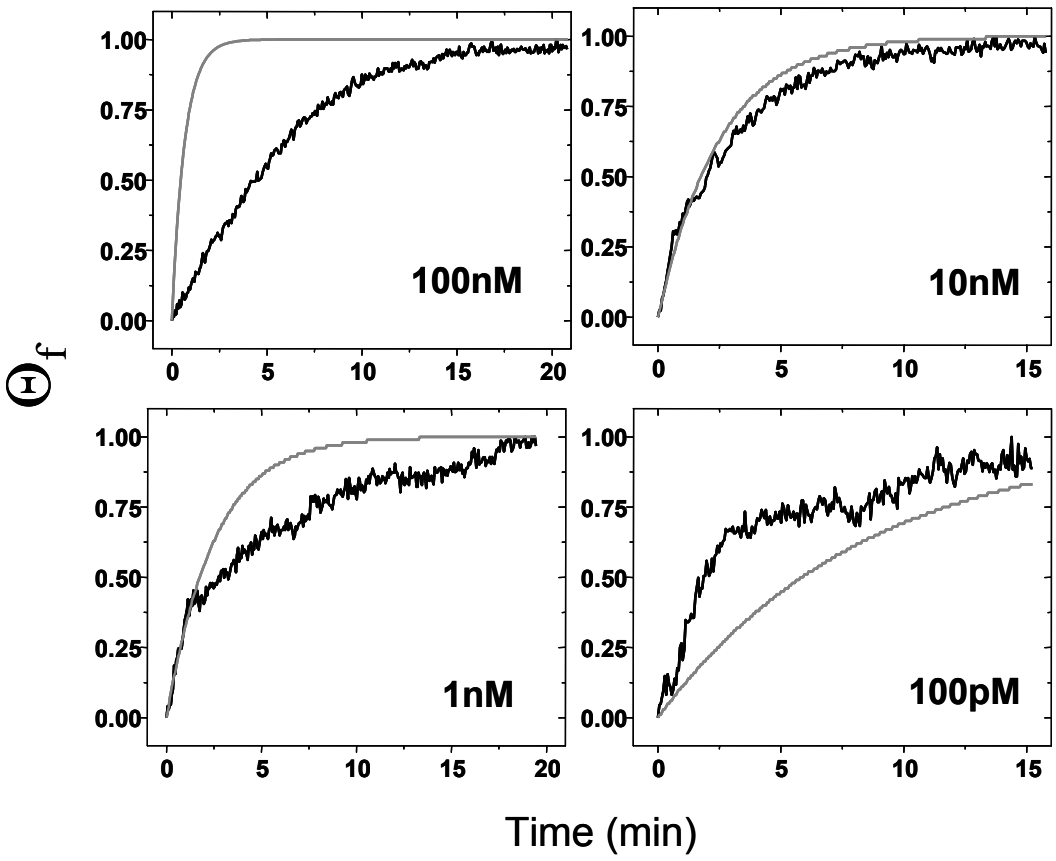

Figure 3.17: Graphical representation of equation 3.19 (Θ_f) using the kinetic parameters obtained from the SPR experiments (1x PBS) (κ_{on}=4.71e5 $M^{-1}s^{-1}$ and κ_{off}=1.92e-3 s^{-1}) (grey curves) and SiNW resistance versus time data (10μM PBS) (black curves) for four concentrations of IL2. Time zero is the time when pure 10μM PBS was switched to a solution containing indicated concentrations of IL2.

We now attempt to use the above derivation, particularly eq. (3.19), to extract kinetic parameters and analyte concentrations from the SiNW sensing data shown in Figure 3.14A. We first qualitatively compare Langmuir model (right side of eq. 3.19) with the SiNW data (left side of eq. 3.19) (Figure 3.17). Kinetic parameters obtained from SPR experiments (Figure 3.14B), κ_{on}=4.71e5 $M^{-1}s^{-1}$ and κ_{off}=1.92e-3 s^{-1}, were used. As Figure 3.17 depicts, there are significant deviations between the Langmuir 1:1 model (grey curves) and SiNW data (black curves). Of course this comparison is purely

qualitative, and merely serves as a guide. Several major differences exist between the SPR and SiNW experiments, which may have resulted in the discrepancies observed in Figure 3.17. First, the SPR experiments were carried out in 1x PBS (0.14M), while nanowire experiments were carried out in 10μM PBS. We attempted to perform SPR experiments in 10μM PBS; however, the data was highly irregular and irreproducible. Therefore, it is probable that the kinetic parameters are affected by the salt concentration, and may vary between the two sets of experiments. The second important different has to do with the surface area of the sensor. The surface area of a SiNW sensor is ~10^{-12} m^2 (ten nanowires), while that of the SPR sensor chip is significantly larger. If we assume the same probe surface density for the two experiments, the number of antibodies available for analyte capture in the case of SPR is much higher. In contrast, fewer surface probes on the surface of SiNWs may lead to "noisier" signal, with larger signal variance.

We can further extract kinetic parameters from the electrical measurements alone, also using eq. (3.19). The decaying part of the curve in Figure 3.14A (when only buffer is flowing and the surface is initially saturated with the analyte) should follow the relation:

$$\Theta_f = \frac{\ln\left(\frac{R}{R_0}\right)}{\ln\left(\frac{R_{sat}}{R_0}\right)} = e^{-\kappa_{off} t} \qquad (3.21)$$

Thus, it is possible to determine the κ_{off} from the decaying part of the sensing data, and then use the obtained value to determine $\kappa_{on}C$ from eq. (3.19). If the concentration (C) or

κ_{on} is known, the other parameter may be readily obtained. Taking the log of both sides of eq. (3.21) yields:

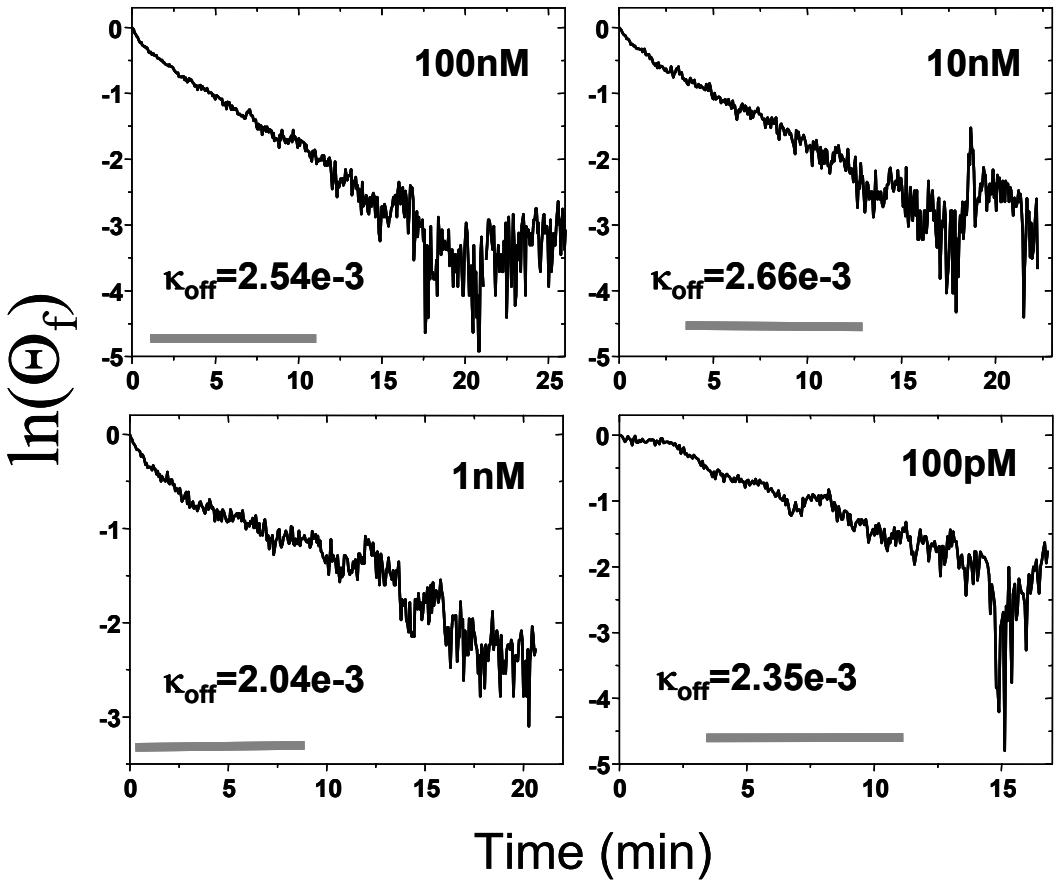

Figure 3.18: Equation (3.22) plotted for different concentrations of IL2 using the data obtained with SiNW experiment during the removal of bound analyte with pure 10μM PBS solution. The parts of the data outlined with grey bars were used for linear regression analysis, which yielded slopes (κ_{off}) indicated on the graphs. Time zero is the time when the solution containing IL2 was switched to 10μM PBS.

$$\ln\left(\frac{\ln\left(\frac{R}{R_0}\right)}{\ln\left(\frac{R_{sat}}{R_0}\right)}\right) = -\kappa_{off} t \qquad (3.22)$$

Since we have a large sample of resistance (R) values versus time, we can utilize linear regression analysis to obtain 95% confidence interval for the κ_{off} value for each IL2 concentration. Figure 3.18 shows eq. (3.22) plotted using the SiNW experimental data obtained for different concentrations of IL2. The κ_{off} values indicated are quite close to the off rate obtained with SPR, 1.92e-3 s^{-1}. Table 3.4 summarizes the results of linear regression of the data in Figure 3.18, including the R^2 values and the 95% confidence intervals of κ_{off} values for different analyte concentrations. We now use the off-rate values obtained above to determine the κ_{on} and the concentration of the analyte. Equation (3.19) can be rearranged to yield:

$$-\kappa_{on} Ct = \ln\left(1 - \frac{\ln\left(\frac{R}{R_0}\right)}{\ln\left(\frac{R_{sat}}{R_0}\right)}\right) + \kappa_{off} t = \Gamma(t) \qquad (3.23)$$

Using the appropriate κ_{off} values, $\Gamma(t)$, defined in eq. (3.23), may be graphed versus the negative values of $\kappa_{on}Ct$ (Figure 3.19). Again, regression analysis yields the values of κ_{on} if we assume that we know exactly the concentration of the analyte. Table 3.4 summarizes the κ_{on} values obtained in this manner as well as the apparent concentration of analyte assuming the κ_{on} value from the SPR experiment. In the range of 1nM to 10nM, the estimated kinetic parameters and apparent analyte concentrations are quite close to real concentrations and the SPR kinetic parameters. However, obvious discrepancies are observed for the 100nM and 100pM IL2 concentrations. Figure 3.17 suggests that serious discrepancies, particularly at these concentrations, should occur, but the origin of such deviations is not obvious. While the off-rates are quite close to the

SPR value at all concentrations, the forward rate, κ_{on}, is significantly slower for the 100nM and significantly higher for 100pM than what is predicted with the Langmuir

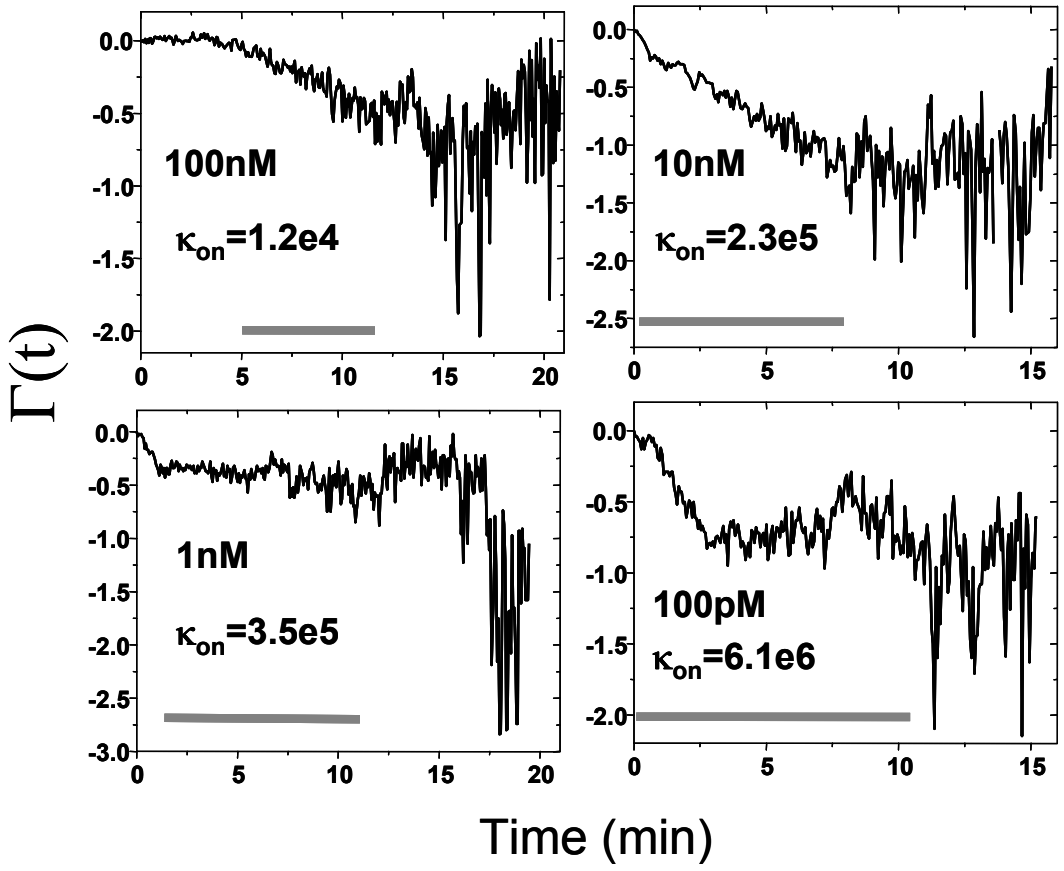

Figure 3.19: Equation (3.23) plotted using the data obtained from the SiNW experiment while flowing 10μM PBS solution containing different concentrations of IL2. The parts of the data outlined with grey bars were used for linear regression analysis, which yielded slopes ($\kappa_{on}C$) that were divided by appropriate known concentrations to obtain κ_{on} values indicated on the graphs. Time zero is the time when the 10μM PBS was switched to 10μM PBS containing IL2.

model and observed by the SPR (Table 3.4). It is possible that at high analyte concentrations in dilute buffer (10μM PBS), protein-protein interactions become significant and compete with antibody-protein interactions, causing the κ_{on} to be underestimated. At very low concentrations, inherently "noisy" measurements due to small surface area of the sensor and the low abundance of the analyte may lead to

nM	K_{off} X10^{-3} (s^{-1})	95% CI		R^2	K_{on} X10^5 ($M^{-1}s^{-1}$)	95% CI		R^2	C (nM)	95% CI		K_A x10^8 (M^{-1})
100	**2.54**	2.49	2.59	0.98	**0.12**	0.11	0.13	0.82	**2.52**	2.31	2.74	**0.047**
10	**2.66**	2.56	2.75	0.94	**2.32**	2.22	2.41	0.94	**4.92**	4.71	5.12	**0.87**
1	**2.04**	1.94	2.14	0.92	**3.48**	2.76	4.19	0.33	**0.74**	0.59	0.89	**1.71**
0.1	**2.35**	2.22	2.47	0.91	**60.5**	45.2	75.8	0.24	**1.29**	0.96	1.61	**25.7**
SPR	**1.9**				**4.71**							**2.45**

Table 3.4: Kinetic parameters calculated from linear regression analysis of the SiNW sensing data for four analyte concentrations (equations 3.22 and 3.23). The 95% confidence intervals are included. Concentrations of the analyte (C) are obtained by using the SPR κ_{on} value, while the SiNW κ_{on} values are obtained by using the known analyte concentrations. For comparison, the kinetic parameters obtained from the SPR experiment are also presented.

significant deviations from the Langmuir model. It is, however, very encouraging that the method derived above yields meaningful values of the kinetic parameters and accurate analyte concentrations in the range between 100nM and 100pM. Further theoretical and experimental work is needed to determine the reasons for the deviations of SiNW sensing data from the Langmuir binding model.

3.6 Discussion

Real-time and label-free detection of DNA 16-mers and proteins with SiNWs was performed. Primary DNA was electrostatically adsorbed onto an amine-terminated SiNW surface and hybridized to the complementary strand in a microfluidics channel under flow. Electrostatic adsorption of single-stranded DNA to poly-L-lysine coated surface has previously been electronically detected at nanomolar concentrations with capacitive methods on lowly doped Si electrodes in 0.015M solution.[58] The ability to

detect DNA under physiological conditions and at a detection limit of 1fM, as demonstrated in this work, is of significance as it may allow the direct use of biological samples such as serum or tissue culture media. It is likely that because the primary DNA is electrostatically bound and hybridization occurs very close to NW surface, Debye screening does not prevent SiNW based detection. We attempted to carry out hybridization in pure water; however, no changes in SiNW resistance were observed (data not shown), presumably because DNA-DNA repulsion is significant in that case.

SiNWs with significantly reduced oxide coverage exhibited enhanced solution FET characteristics (Figure 3.5) when compared to SiNWs characterized by a native SiO_2 surface passivation. Oxide covered, highly doped SiNWs were designed to exhibit a similar dynamic range of DNA detection as the best near-infrared imaging SPR technique[62]-10nM for 18-mer, corresponding to ~10^{11} molecules/cm^2. When identical nanowires were functionalized by the UV-initiated radical chemistry method, resulting in near-elimination of the Si-SiO_2 interface, the limit of detection was increased by two orders of magnitude, with an accompanying increase in the dynamic range. This result highlights the importance of controlling surface chemistry of SiNWs for their optimization as biological sensors. In the future, surface chemistries yielding higher coverage than UV-initiated alkylation may be utilized to passivate and electrochemically convert SiNWs into arrays for multiparameter analysis.[38, 63]

Sensing of an important cytokine, interleukin-2, has also been performed. Protein detection is significantly limited by the size of the capture agent. Using antibodies poses a limitation on the ionic strength of the buffer containing the analyte. To circumvent this limitation, aptamers and small peptides must be developed as alternative high-affinity protein probes. However, a combination of an appropriate doping level and surface

chemistry will undoubtedly allow the detection down to a subpicomolar regime, which is more than sufficient for most relevant clinical applications.

Finally, a model that is consistent with both the standard Langmuir binding model and with the fundamentals of semiconductor physics is developed. Kinetic parameters and analyte concentrations that are consistent with SPR values may be extracted from the silicon nanowire experiments. The potential for SiNW sensors to quantitate the concentrations of low-abundance biomolecules within physiological relevant environments is an intriguing one, and we are currently vigorously pursuing this possibility. The most useful application of our model would be in extracting otherwise unknown concentration values once κ_{on} and κ_{off} values are known. As demonstrated here, SiNW sensors can be used for label-free biomolecule detection at concentrations significantly below the limits of detection for SPR. The robustness of the fabrication technique (SNAP) employed here, which yields nanowire sensors that exhibit reproducible and highly tunable behavior, holds a promise for the future integration of this technology within the clinical setting.

Bibliography

1. Kong, J.; Franklin, N. R.; Zhou, C. W.; Chapline, M. G.; Peng, S.; Cho, K. J.; Dai, H. J., Nanotube molecular wires as chemical sensors. *Science* **2000,** 287, (5453), 622-625.
2. Patolsky, F.; Timko, B. P.; Zheng, G. F.; Lieber, C. M., Nanowire-based nanoelectronic devices in the life sciences. *MRS Bulletin* **2007,** 32, (2), 142-149.
3. Park, S. J.; Taton, T. A.; Mirkin, C. A., Array-based electrical detection of DNA with nanoparticle probes. *Science* **2002,** 295, (5559), 1503-1506.
4. Ziegler, C., Nanotechnologies for the biosciences. *Anal. Bioanal. Chem.* **2004,** 379, (7-8), 903-903.
5. Lasseter, T. L.; Cai, W.; Hamers, R. J., Frequency-dependent electrical detection of protein binding events. *Analyst* **2004,** 129, (1), 3-8.
6. Davidson, E. H.; Rast, J. P.; Oliveri, P.; Ransick, A.; Calestani, C.; Yuh, C. H.; Minokawa, T.; Amore, G.; Hinman, V.; Arenas-Mena, C.; Otim, O.; Brown, C. T.; Livi, C. B.; Lee, P. Y.; Revilla, R.; Rust, A. G.; Pan, Z. J.; Schilstra, M. J.; Clarke, P. J. C.; Arnone, M. I.; Rowen, L.; Cameron, R. A.; McClay, D. R.; Hood, L.; Bolouri, H., A genomic regulatory network for development. *Science* **2002,** 295, (5560), 1669-1678.
7. Kitano, H., Systems biology: A brief overview. *Science* **2002,** 295, (5560), 1662-1664.
8. Hood, L.; Heath, J. R.; Phelps, M. E.; Lin, B. Y., Systems biology and new technologies enable predictive and preventative medicine. *Science* **2004,** 306, (5696), 640-643.
9. Chen, R. J.; Bangsaruntip, S.; Drouvalakis, K. A.; Kam, N. W. S.; Shim, M.; Li, Y. M.; Kim, W.; Utz, P. J.; Dai, H. J., Noncovalent functionalization of carbon nanotubes for highly specific electronic biosensors. *Proc. Nat. Acad. Sci.* USA **2003,** 100, (9), 4984-4989.
10. Star, A.; Tu, E.; Niemann, J.; Gabriel, J. C. P.; Joiner, C. S.; Valcke, C., Label-free detection of DNA hybridization using carbon nanotube network field-effect transistors. *Proc. Nat. Acad. Sci.* USA **2006,** 103, (4), 921-926.
11. Besteman, K.; Lee, J. O.; Wiertz, F. G. M.; Heering, H. A.; Dekker, C., Enzyme-coated carbon nanotubes as single-molecule biosensors. *Nano Lett.* **2003,** 3, (6), 727-730.
12. Maehashi, K.; Katsura, T.; Kerman, K.; Takamura, Y.; Matsumoto, K.; Tamiya, E., Label-free protein biosensor based on aptamer-modified carbon nanotube field-effect transistors. *Anal. Chem.* **2007,** 79, (2), 782-787.
13. Cui, Y.; Wei, Q. Q.; Park, H. K.; Lieber, C. M., Nanowire nanosensors for highly sensitive and selective detection of biological and chemical species. *Science* **2001,** 293, (5533), 1289-1292.
14. Hahm, J.; Lieber, C. M., Direct ultrasensitive electrical detection of DNA and DNA sequence variations using nanowire nanosensors. *Nano Lett.* **2004,** 4, (1), 51-54.

15. Li, Z.; Chen, Y.; Li, X.; Kamins, T. I.; Nauka, K.; Williams, R. S., Sequence-specific label-free DNA sensors based on silicon nanowires. *Nano Lett.* **2004,** 4, (2), 245-247.
16. Li, C.; Curreli, M.; Lin, H.; Lei, B.; Ishikawa, F. N.; Datar, R.; Cote, R. J.; Thompson, M. E.; Zhou, C. W., Complementary detection of prostate-specific antigen using ln(2)O(3) nanowires and carbon nanotubes. *J. Am. Chem. Soc.* **2005,** 127, (36), 12484-12485.
17. Ramanathan, K.; Bangar, M. A.; Yun, M.; Chen, W.; Myung, N. V.; Mulchandani, A., Bioaffinity sensing using biologically functionalized conducting-polymer nanowire. *J. Am. Chem. Soc.* **2005,** 127, (2), 496-497.
18. Lud, S. Q.; Nikolaides, M. G.; Haase, I.; Fischer, M.; Bausch, A. R., Field effect of screened charges: Electrical detection of peptides and proteins by a thin-film resistor. *Chemphyschem* **2006,** 7, (2), 379-384.
19. Neff, P. A.; Wunderlich, B. K.; Lud, S. Q.; Bausch, A. R., Silicon-on-insulator based thin film resistors for quantitative biosensing applications. *Physica Status Solidi A* **2006,** 203, (14), 3417-3423.
20. Israelachvilli, J., *Intermolecular and Surface Forces*. London: Academic Press, 1985.
21. Zheng, G. F.; Patolsky, F.; Cui, Y.; Wang, W. U.; Lieber, C. M., Multiplexed electrical detection of cancer markers with nanowire sensor arrays. *Nat. Biotechnol.* **2005,** 23, (10), 1294-1301.
22. Okahata, Y.; Kawase, M.; Niikura, K.; Ohtake, F.; Furusawa, H.; Ebara, Y., Kinetic measurements of DNA hybridisation an an oligonucleotide-immobilized 27-MHz quartz crystal microbalance. *Anal. Chem.* **1998,** 70, (7), 1288-1296.
23. Li, Z.; Rajendran, B.; Kamins, T. I.; Li, X.; Chen, Y.; Williams, R. S., Silicon nanowires for sequence-specific DNA sensing: device fabrication and simulation. *Appl. Phys. A* **2005,** 80, (6), 1257-1263.
24. Vieu, C.; Carcenac, F.; Pepin, A.; Chen, Y.; Mejias, M.; Lebib, A.; Manin-Ferlazzo, L.; Couraud, L.; Launois, H., Electron beam lithography: resolution limits and applications. *Appl. Surf. Sci.* **2000,** 164, 111-117.
25. Yang, P. D., The chemistry and physics of semiconductor nanowires. *MRS Bulletin* **2005,** 30, (2), 85-91.
26. Stern, E.; Klemic, J. F.; Routenberg, D. A.; Wyrembak, P. N.; Turner-Evans, D. B.; Hamilton, A. D.; LaVan, D. A.; Fahmy, T. M.; Reed, M. A., Label-free immunodetection with CMOS-compatible semiconducting nanowires. *Nature* **2007,** 445, (7127), 519-522.
27. Gao, Z.; Agarwal, A.; Trigg, A. D.; Singh, N.; Fang, C.; Tung, C. H.; Fan, Y.; Buddharaju, K. D.; Kong, J., Silicon nanowire arrays for label-free detection of DNA. *Anal. Chem.* **2007**.
28. Heath, J. R.; Legoues, F. K., A liquid solution synthesis of single-crystal germanium quantum wires. *Chem. Phys. Lett.* **1993,** 208, (3-4), 263-268.
29. Morales, A. M.; Lieber, C. M., A laser ablation method for the synthesis of crystalline semiconductor nanowires. *Science* **1998,** 279, (5348), 208-211.
30. Chung, S. W.; Yu, J. Y.; Heath, J. R., Silicon nanowire devices. *Appl. Phys. Lett.* **2000,** 76, (15), 2068-2070.

31. Melosh, N. A.; Boukai, A.; Diana, F.; Gerardot, B.; Badolato, A.; Petroff, P. M.; Heath, J. R., Ultrahigh-density nanowire lattices and circuits. *Science* **2003,** 300, (5616), 112-115.
32. Beckman, R. A.; Johnston-Halperin, E.; Melosh, N. A.; Luo, Y.; Green, J. E.; Heath, J. R., Fabrication of conducting Si nanowire arrays. *J. Appl. Phys.* **2004,** 96, (10), 5921-5923.
33. Wikswo, J. P.; Prokop, A.; Baudenbacher, F.; Cliffel, D.; Csukas, B.; Velkovsky, M., Engineering challenges of BioNEMS: the integration of microfluidics, micro- and nanodevices, models and external control for systems biology. *IEE Proc.-Nanobiotechnol.* **2006,** 153, (4), 81-101.
34. Yablonovitch, E.; Allara, D. L.; Chang, C. C.; Gmitter, T.; Bright, T. B., Unusually low surface-recombination velocity on silicon and germanium surfaces. *Phys. Rev. Lett.* **1986,** 57, (2), 249-252.
35. Sham, T. K.; Naftel, S. J.; Kim, P. S. G.; Sammynaiken, R.; Tang, Y. H.; Coulthard, I.; Moewes, A.; Freeland, J. W.; Hu, Y. F.; Lee, S. T., Electronic structure and optical properties of silicon nanowires: A study using x-ray excited optical luminescence and x-ray emission spectroscopy. *Phys. Rev. B* **2004,** 70, (4).
36. Webb, L. J.; Lewis, N. S., Comparison of the electrical properties and chemical stability of crystalline silicon(111) surfaces alkylated using grignard reagents or olefins with Lewis acid catalysts. *J. Phys. Chem. B* **2003,** 107, (23), 5404-5412.
37. Bansal, A.; Lewis, N. S., Stabilization of Si photoanodes in aqueous electrolytes through surface alkylation. *J. Phys. Chem. B* **1998,** 102, (21), 4058-4060.
38. Bunimovich, Y. L.; Ge, G. L.; Beverly, K. C.; Ries, R. S.; Hood, L.; Heath, J. R., Electrochemically programmed, spatially selective biofunctionalization of silicon wires. *Langmuir* **2004,** 20, (24), 10630-10638.
39. Haick, H.; Hurley, P. T.; Hochbaum, A. I.; Yang, P. D.; Lewis, N. S., Electrical characteristics and chemical stability of non-oxidized, methyl-terminated silicon nanowires. *J. Am. Chem. Soc.* **2006,** 128, (28), 8990-8991.
40. Terry, J.; Mo, R.; Wigren, C.; Cao, R. Y.; Mount, G.; Pianetta, P.; Linford, M. R.; Chidsey, C. E. D., Reactivity of the H-Si (111) surface. *Instrum. Methods Phys. Res., Sect. B* **1997,** 133, (1-4), 94-101.
41. Effenberger, F.; Gotz, G.; Bidlingmaier, B.; Wezstein, M., Photoactivated preparation and patterning of self-assembled monolayers with 1-alkenes and aldehydes on silicon hydride surfaces. *Angew. Chem., Int. Ed.* **1998,** 37, (18), 2462-2464.
42. Boukherroub, R.; Wayner, D. D. M., Controlled functionalization and multistep chemical manipulation of covalently modified Si(111) surfaces. *J. Am. Chem. Soc.* **1999,** 121, (49), 11513-11515.
43. Cicero, R. L.; Linford, M. R.; Chidsey, C. E. D., Photoreactivity of unsaturated compounds with hydrogen-terminated silicon(111). *Langmuir* **2000,** 16, (13), 5688-5695.
44. Streifer, J. A.; Kim, H.; Nichols, B. M.; Hamers, R. J., Covalent functionalization and biomolecular recognition properties of DNA-modified silicon nanowires. *Nanotechnology* **2005,** 16, (9), 1868-1873.
45. Jonsson, U.; Fagerstam, L.; Ivarsson, B.; Johnsson, B.; Karlsson, R.; Lundh, K.; Lofas, S.; Persson, B.; Roos, H.; Ronnberg, I.; Sjolander, S.; Stenberg, E.; Stahlberg, R.; Urbaniczky, C.; Ostlin, H.; Malmqvist, M., Real-time biospecific

interaction analysis using surface-plasmon resonance and a sensor chip technology. *Biotechniques* **1991,** 11, (5), 620-&.

46. Wang, D. W.; Sheriff, B. A.; Heath, J. R., Silicon p-FETs from ultrahigh density nanowire arrays. *Nano Lett.* **2006,** 6, (6), 1096-1100.
47. Duffy, D. C.; McDonald, J. C.; Schueller, O. J. A.; Whitesides, G. M., Rapid prototyping of microfluidic systems in poly(dimethylsiloxane). *Anal. Chem.* **1998,** 70, (23), 4974-4984.
48. Unger, M. A.; Chou, H. P.; Thorsen, T.; Scherer, A.; Quake, S. R., Monolithic microfabricated valves and pumps by multilayer soft lithography. *Science* **2000,** 288, (5463), 113-116.
49. Haber, J. A.; Lewis, N. S., Infrared and X-ray photoelectron spectroscopic studies of the reactions of hydrogen-terminated crystalline Si(111) and Si(100) surfaces with Br-2, I-2, and ferrocenium in alcohol solvents. *J. Phys. Chem. B* **2002,** 106, (14), 3639-3656.
50. Himpsel, F. J.; McFeely, F. R.; Talebibrahimi, A.; Yarmoff, J. A.; Hollinger, G., Microscopic structure of the SiO_2/Si interface. *Phys. Rev. B* **1988,** 38, (9), 6084-6096.
51. Hu, K.; Fan, F. R. F.; Bard, A. J.; Hillier, A. C., Direct measurement of diffuse double-layer forces at the semiconductor/electrolyte interface using an atomic force microscope. *J. Phys. Chem. B* **1997,** 101, (41), 8298-8303.
52. Cui, Y.; Duan, X. F.; Hu, J. T.; Lieber, C. M., Doping and electrical transport in silicon nanowires. *J. Phys. Chem. B* **2000,** 104, (22), 5213-5216.
53. Cheng, M. M.-C.; Cuda, G.; Bunimovich, Y. L.; Gaspari, M.; Heath, J. R.; Hill, H. D.; Mirkin, C. A.; Nijdam, A. J.; Terracciano, R.; Thundat, T.; Ferrari, M., Nanotechnologies for biomolecular detection and medical diagnostics. *Curr. Opin. Chem. Biol.* **2006,** 10, (1), 11-19.
54. Beckman, R.; Johnston-Halperin, E.; Luo, Y.; Green, J. E.; Heath, J. R., Bridging dimensions: Demultiplexing ultrahigh-density nanowire circuits. *Science* **2005,** 310, (5747), 465-468.
55. Stenberg, E.; Persson, B.; Roos, H.; Urbaniczky, C., Quantitative determination of surface concentration of protein with surface-plasmon resonance using radiolabeled proteins. *J. Colloid Interface Sci.* **1991,** 143, (2), 513-526.
56. Yu, F.; Yao, D. F.; Knoll, W., Oligonucleotide hybridization studied by a surface plasmon diffraction sensor (SPDS). *Nucleic Acids Res.* **2004,** 32, (9).
57. Sze, S. M., *Physics of Semiconductor Devices*, 2nd ed., Taipei: John Wiley & Sons, 1981.
58. Fritz, J.; Cooper, E. B.; Gaudet, S.; Sorger, P. K.; Manalis, S. R., Electronic detection of DNA by its intrinsic molecular charge. *Proc. Nat. Acad. Sci.* USA **2002,** 99, (22), 14142-14146.
59. Peterson, A. W.; Heaton, R. J.; Georgiadis, R. M., The effect of surface probe density on DNA hybridization. *Nucleic Acids Res.* **2001,** 29, (24), 5163-5168.
60. Lemeshko, S. V.; Powdrill, T.; Belosludtsev, Y. Y.; Hogan, M., Oligonucleotides form a duplex with non-helical properties on a positively charged surface. *Nucleic Acids Res.* **2001,** 29, (14), 3051-3058.
61. Zimmermann, M.; Delamarche, E.; Wolf, M.; Hunziker, P., Modeling and optimization of high-sensitivity, low-volume microfluidic-based surface immunoassays. *Biomed. Microdevices* **2005,** 7, (2), 99-110.

62. Nelson, B. P.; Grimsrud, T. E.; Liles, M. R.; Goodman, R. M.; Corn, R. M., Surface plasmon resonance imaging measurements of DNA and RNA hybridization adsorption onto DNA microarrays. *Anal. Chem.* **2001,** 73, (1), 1-7.
63. Rohde, R. D.; Agnew, H. D.; Yeo, W. S.; Bailey, R. C.; Heath, J. R., A non-oxidative approach toward chemically and electrochemically functionalizing Si(111). *J. Am. Chem. Soc.* **2006,** 128, (29), 9518-9525.